

Bayesian Multi-task Variable Selection with an Application to Differential DAG Analysis

Guanxun Li and Quan Zhou

Department of Statistics, Texas A&M University

June 30, 2022

Abstract

In this paper, we study the Bayesian multi-task variable selection problem, where the goal is to select activated variables for multiple related data sets simultaneously. Our proposed method generalizes the spike-and-slab prior to multiple data sets, and we prove its posterior consistency in high-dimensional regimes. To calculate the posterior distribution, we propose a novel variational Bayes algorithm based on the recently developed “sum of single effects” model of Wang et al. (2020a). Finally, motivated by differential gene network analysis in biology, we extend our method to joint learning of multiple directed acyclic graphical models. Both simulation studies and real gene expression data analysis are conducted to show the effectiveness of the proposed method.

1 Introduction

In machine learning, multi-task learning refers to the paradigm where we simultaneously learn multiple related tasks instead of learning each task independently (Zhang and Yang, 2021). In the context of model selection, we can formulate the problem as follows: given K observed data sets where the k -th data set is generated from a statistical model $\mathfrak{M}^{(k)}$, simultaneously estimate $\mathfrak{M}^{(1)}, \dots, \mathfrak{M}^{(K)}$ so that the estimation of $\mathfrak{M}^{(k)}$ (for any $k = 1, \dots, K$) utilizes information from all K data sets. In real problems where the K models tend to share many common features, this joint estimation approach is expected to have better performance than separate estimation (i.e., estimating $\mathfrak{M}^{(k)}$ using only the k -th data set). In this work, we consider multi-task learning problems where each $\mathfrak{M}^{(k)}$ may be a variable selection model or a directed acyclic graph.

We first study the multi-task variable selection problem, where each data set is generated from a sparse linear regression model. The majority of the existing research has been conducted under the strict assumption that the “activated” covariates (i.e., covariates with nonzero regression coefficients) are shared across all data sets (Lounici et al., 2009, 2011). Recent works have relaxed this assumption by taking a more adaptable strategy that splits each regression coefficient into a shared and an individual components (Jalali et al., 2010; Hernández-Lobato et al., 2015). We propose a more flexible Bayesian method which generalizes the well-known spike-and-slab prior (George and McCulloch, 1993; Ishwaran and Rao, 2005) and allows a covariate to be activated in an arbitrary number of data sets with varying effect sizes. We prove the posterior consistency for our

model in high-dimensional scenarios. While there is a large literature on frequentists’ approaches to multi-task learning, the corresponding Bayesian methodology has received less attention and in particular theoretical results are lacking (Bonilla et al., 2007; Guo et al., 2011; Hernández-Lobato et al., 2015). To our knowledge, this is the first work that establishes the theoretical guarantees for the high-dimensional Bayesian multi-task variable selection problem.

The traditional method for obtaining the posterior distribution for a Bayesian model is to use Markov Chain Monte Carlo (MCMC) sampling, which is often computationally intensive, especially for multi-task learning problems where the space of candidate models can be enormous. A more scalable alternative is variational Bayes (VB), which recasts posterior approximation as an optimization problem (Ray and Szabó, 2021). To carry out efficient VB inference, we approximate our spike-and-slab prior model using a novel multi-task sum of single effects (muSuSiE) model, which extends the sum of single effects (SuSiE) model of Wang et al. (2020a) to multiple data sets. Then, we propose to fit muSuSiE using an iterative Bayesian stepwise selection (IBSS) method, which may be thought of as a coordinate ascent algorithm for maximizing the evidence lower bound (ELBO) over a particular variational family.

To illustrate the application of the proposed methodology to more complex multi-task learning problems, we consider differential network analysis based on directed acyclic graphs (DAGs), an important topic in biology that has gained increasing interest in recent years (Li et al., 2020; Shojaie, 2021); this is essentially a multi-task structure learning problem. Because learning a DAG model can be equivalently viewed as a set of variable selection problems when the order of nodes is known (Agrawal et al., 2018), learning multiple DAG models with a known order is likewise equivalent to a set of multi-task variable selection problems. However, when the order is not known (which is usually the case in practice), learning the order of nodes from the data can be very challenging. To overcome this issue, we employ MCMC sampling over the permutation space to average over the uncertainty in learning the order of nodes and then compute the DAG model for each given order via the proposed Bayesian multi-task variable selection approach. Simulation studies and a real data example are used to demonstrate the effectiveness of the proposed method.

The rest of this paper is organized as follows. In Section 2, we introduce our Bayesian multi-task variable selection model, prove the high-dimensional posterior consistency and describe the VB algorithm for model-fitting. Section 3 presents simulation results for the multi-task variable selection problem. In Section 4, we generalize our method to joint estimation of multiple DAG models and propose an order MCMC sampler. Simulation studies and real data analysis for differential DAG analysis are presented in Sections 5 and 6, respectively. Section 7 concludes the paper with a brief discussion. Proofs, additional simulation results and more details about the algorithm implementation are deferred to the appendices.

2 Bayesian Multi-task Variable Selection

2.1 Model, prior and posterior distributions

For any index vector $\mathbf{r} \in \{0, 1\}^p$, denote $S_{\mathbf{r}} = \{j \in [p] : r_j = 1\}$, where $[p] = \{1, \dots, p\}$. For any vector \mathbf{b} and matrix \mathbf{A} , let $\mathbf{b}_{\mathbf{r}}$ be the subvector of \mathbf{b} with index set $S_{\mathbf{r}}$ and $\mathbf{A}_{\mathbf{r}}$ be the submatrix of \mathbf{A} containing columns indexed by $S_{\mathbf{r}}$. Similarly, $\mathbf{b}_{\mathbf{r}^c}$ denotes the subvector with index set $S_{\mathbf{r}}^c = [p] \setminus S_{\mathbf{r}}$, and $\mathbf{A}_{\mathbf{r}^c}$ denotes the submatrix with columns indexed by $S_{\mathbf{r}}^c$. For a set S , we use $|S|$ to denote its cardinality, and for a vector $\mathbf{r} \in \{0, 1\}^p$, we let $|\mathbf{r}| = \sum_{i=1}^p r_i$; thus, we have $|\mathbf{r}| = |S_{\mathbf{r}}|$. Let \mathcal{P}_K be

the power set of $[K]$ excluding the empty set.

Let K denote the number of data sets we have, which is treated as fixed throughout this paper. For the k -th data set, let $\mathbf{y}^{(k)} \in \mathbb{R}^{n_k}$ denote the response data, and $\mathbf{X}^{(k)} \in \mathbb{R}^{n_k \times p}$ denote the design matrix containing n_k observations of p explanatory variables (we assume the p predictors are observed in all K data sets). Consider the linear regression model

$$\mathbf{y}^{(k)} = \mathbf{X}^{(k)}\boldsymbol{\beta}^{(k)} + \mathbf{e}^{(k)}, \quad \text{where } \mathbf{e}^{(k)} \sim \mathcal{N}_{n_k}(0, \sigma_{(k)}^2 \mathbf{I}_{n_k}), \quad (1)$$

where \mathcal{N}_n denotes the n -dimensional normal distribution, \mathbf{I}_n denotes the n -dimensional identity matrix, and the vector of regression coefficients, $\boldsymbol{\beta}^{(k)}$, is assumed to be sparse. For now, we assume that the error variance $\sigma_{(k)}^2$ is known, and we will explain in Appendix B how to estimate it in practice. As in the spike-and-slab variable selection, we introduce the indicator vector $\mathbf{r}^{(k)} \in \{0, 1\}^p$ such that $r_j^{(k)} = 1$ means $\beta_j^{(k)}$ is nonzero. We say the j -th covariate is activated in the k -th data set if $r_j^{(k)} = 1$. Hence, $|\mathbf{r}^{(k)}|$ is the number of activated covariates in the k -th data set. We put the following conditional prior on $\{\boldsymbol{\beta}^{(k)}\}_{k=1}^K$:

$$\begin{aligned} \boldsymbol{\beta}^{(1)}, \dots, \boldsymbol{\beta}^{(K)} \text{ are independent given } \mathbf{r}^{(1)}, \dots, \mathbf{r}^{(K)}, \text{ and} \\ \boldsymbol{\beta}_{\mathbf{r}^{(k)}}^{(k)} | \mathbf{r}^{(k)} \sim \mathcal{N}_{|\mathbf{r}^{(k)}|}(0, \boldsymbol{\Sigma}_{0(k)}), \text{ where } \boldsymbol{\Sigma}_{0(k)} = \text{diag}(\sigma_{01(k)}^2, \dots, \sigma_{0|\mathbf{r}^{(k)}|(k)}^2), \end{aligned} \quad (2)$$

where the hyperparameters $\{\sigma_{0l(k)}^2 : l = 1, \dots, |\mathbf{r}^{(k)}|\}$ are allowed to be different. Write $\mathbf{r} = (\mathbf{r}^{(k)})_{k=1}^K$, and define our model space by

$$\mathbb{M}_{\mathbf{r}} = \left\{ \mathbf{r} \in \{0, 1\}^{pK} : \left| \left\{ j \in [p] : \sum_{k=1}^K r_j^{(k)} \geq 1 \right\} \right| \leq L \right\}, \quad (3)$$

where the hyperparameter L gives the maximum number of activated covariates (in at least one data set) we allow. It will be sometimes convenient to reparameterize \mathbf{r} using another indicator vector $\boldsymbol{\gamma} \in \{0, 1\}^{p|\mathcal{P}_K|}$, where $|\mathcal{P}_K| = 2^K - 1$ by the definition of \mathcal{P}_K . Partition $\boldsymbol{\gamma}$ by $\boldsymbol{\gamma} = (\boldsymbol{\gamma}^I)_{I \in \mathcal{P}_K}$, where $\boldsymbol{\gamma}^I \in \{0, 1\}^p$ for each $I \in \mathcal{P}_K$, and for each $j \in [p]$, define

$$\gamma_j^I = \begin{cases} 1, & \text{if } I = \{k \in [K] : r_j^{(k)} = 1\}, \\ 0, & \text{otherwise.} \end{cases} \quad (4)$$

That is, $\gamma_j^I = 1$ if and only if the j -th covariate is activated in the data sets indexed by I and deactivated in all the other data sets; this implies that for any $I \neq I'$, γ_j^I and $\gamma_j^{I'}$ cannot both be 1. Denote this mapping by $\boldsymbol{\gamma}(\mathbf{r})$ and define

$$\mathbb{M}_{\boldsymbol{\gamma}} = \{\boldsymbol{\gamma}(\mathbf{r}) : \mathbf{r} \in \mathbb{M}_{\mathbf{r}}\}. \quad (5)$$

Note that for any $\boldsymbol{\gamma} \in \mathbb{M}_{\boldsymbol{\gamma}}$, we have $|\boldsymbol{\gamma}| \leq L$, since $|\boldsymbol{\gamma}|$ gives the number of unique covariates that are activated in at least one data set. Given $\boldsymbol{\gamma} \in \mathbb{M}_{\boldsymbol{\gamma}}$, we can obtain \mathbf{r} by

$$\mathbf{r}^{(k)} = \sum_{I \in \mathcal{I}_k} \boldsymbol{\gamma}^I, \quad \text{where } \mathcal{I}_k = \{I \in \mathcal{P}_K : k \in I\}. \quad (6)$$

Below is an example for $K = 2$.

Example 1. When $K = 2$, $\mathbf{r} = (\mathbf{r}^{(1)}, \mathbf{r}^{(2)}) \in \{0, 1\}^{2p}$ and $\boldsymbol{\gamma} = (\boldsymbol{\gamma}^{\{1\}}, \boldsymbol{\gamma}^{\{2\}}, \boldsymbol{\gamma}^{\{1,2\}}) \in \{0, 1\}^{3p}$. Given $\mathbf{r} \in \mathbb{M}_{\mathbf{r}}$, $\gamma_j^{\{1\}} = 1$ if and only if $r_j^{(1)} = 1$ and $r_j^{(2)} = 0$, and $\gamma_j^{\{1,2\}} = 1$ if and only if $r_j^{(1)} = r_j^{(2)} = 1$. Given $\boldsymbol{\gamma} \in \mathbb{M}_{\boldsymbol{\gamma}}$, we can recover \mathbf{r} by $\mathbf{r}^{(1)} = \boldsymbol{\gamma}^{\{1\}} + \boldsymbol{\gamma}^{\{1,2\}}$ and $\mathbf{r}^{(2)} = \boldsymbol{\gamma}^{\{2\}} + \boldsymbol{\gamma}^{\{1,2\}}$.

Let $\mathcal{M}_j = \{k \in [K]: r_j^{(k)} = 1\}$ be the index set of the data sets where the j -th covariate is activated and $m_j = |\mathcal{M}_j|$. We consider the following prior distribution on $\boldsymbol{\gamma}$, which induces a prior on \mathbf{r} :

$$\Pi(\boldsymbol{\gamma}) \propto \mathbb{1}\{\boldsymbol{\gamma} \in \mathbb{M}_{\boldsymbol{\gamma}}\} f(|\boldsymbol{\gamma}|, L) \prod_{k=1}^K p^{-\omega_k \sum_{j \in [p]} \mathbb{1}\{m_j=k\}}, \quad (7)$$

where $\mathbb{1}$ is the indicator function. The function $f(|\boldsymbol{\gamma}|, L)$ is assumed to be “asymptotically negligible” compared with the product term in (7) and will be specified later. The hyperparameters $\{\omega_k\}_{k=1}^K$ penalize models with larger sizes, where ω_k can be seen as the “cost” we pay for activating one covariate simultaneously in k data sets. For most multi-task variable selection problems in reality, it is reasonable to assume that activated covariates tend to be shared across data sets, and to reflect this prior belief, we propose to choose $\{\omega_k\}_{k=1}^K$ such that

$$\frac{\omega_K}{K} < \frac{\omega_{K-1}}{K-1} < \frac{\omega_{K-2}}{K-2} < \cdots < \frac{\omega_2}{2} < \omega_1. \quad (8)$$

To see the reasoning behind (8), consider the case $K = 2$ where the above condition is reduced to $\omega_2 < 2\omega_1$. Suppose that the first two covariates are identical in both data sets, and consider two models $\boldsymbol{\gamma}, \boldsymbol{\gamma}'$ where $\gamma_1^{\{1\}} = \gamma_2^{\{2\}} = (\boldsymbol{\gamma}')_1^{\{1,2\}} = 1$ and all other entries of $\boldsymbol{\gamma}, \boldsymbol{\gamma}'$ are 0. Then, $\boldsymbol{\gamma}, \boldsymbol{\gamma}'$ have the same marginal likelihood, and $\omega_2 < 2\omega_1$ ensures that we favor $\boldsymbol{\gamma}'$. An analogous argument for the general case with $K \geq 2$ leads to (8). Note that the choice of $\omega_1, \dots, \omega_K$ only reflects the experimenter’s prior belief on $\boldsymbol{\gamma}$, and one can even use $\omega_k \ll \omega_1$ for all $k \geq 2$ if prior information reveals that the majority of activated covariates must be shared in multiple data sets. However, in all of our numerical studies, we only use $\{\omega_k\}_{k=1}^K$ such that $\omega_1 \leq \omega_2 \leq \cdots \leq \omega_K$, which appears to be a natural condition in situations where not much prior information is available. We will refer to the model specified by Equations (1) to (7) as μSSVS (multi-task Spike-and-Slab Variable Selection).

2.2 Posterior Consistency for Multi-task Spike-and-slab Variable Selection

In this section, we prove the posterior consistency for the μSSVS model, which generalizes the existing results for a single variable selection problem (Johnson and Rossell, 2012; Narisetty and He, 2014; Yang et al., 2016; Jeong and Ghosal, 2021). For ease of presentation, we only consider the special case $n_k = n$, $\sigma_{(k)}^2 = \sigma^2$ and $\sigma_{0l(k)}^2 = \sigma_0^2$ for $k = 1, \dots, K$ and $l = 1, \dots, |\mathbf{r}^{(k)}|$. In the general case, one can assume boundedness of $\{\sigma_{0l(k)}^2\}_{k,l}$ and then use the same argument to prove the posterior consistency.

Suppose the data is generated by (1) with $\boldsymbol{\beta}^{(k)*}$ being the vector of true regression coefficients for the k -th data set. Our goal is to show that covariates with a relatively high signal strength (aggregated over multiple data sets) can be recovered with high probability. To this end, define the “true” model $\{\mathbf{r}^{(k)*}\}_{k \in [K]}$ as follows. Let $C_{\beta,1}, \dots, C_{\beta,K}$ be constants that depend on n, p, σ^2 and

σ_0^2 . For each j , define

$$m_j^* = \max \left\{ m \in [K]: \sum_{k \in [K]} \mathbb{1} \left\{ (\beta_j^{(k)*})^2 \geq C_{\beta, m} \right\} = m \right\},$$

and set $r_j^{(k)*} = 1$ if and only if $(\beta_j^{(k)*})^2 \geq C_{\beta, m_j^*}$, in which case we say the j -th covariate is “influential” in the k -th data set (a “non-influential” covariate may have a small but nonzero regression coefficient). In words, $C_{\beta, k}$ can be seen as the detection threshold for covariates that have relatively large nonzero regression coefficients in k data sets. For our posterior consistency result, we will assume that $C_{\beta, 1} > \dots > C_{\beta, K}$, which reflects the advantage of multi-task learning: if a covariate is activated in more data sets, the signal size in each data set required for detection can be smaller. Let $\boldsymbol{\gamma}^* = (\boldsymbol{\gamma}^{I*})_{I \in \mathcal{P}_K} = \boldsymbol{\gamma}(\mathbf{r}^*)$, where the mapping $\boldsymbol{\gamma}(\mathbf{r})$ is defined in (4).

We assume the following five conditions hold for $k = 1, \dots, K$, which were also used in the consistency analysis for the single variable selection problem conducted in Yang et al. (2016). But since we use an independent normal prior on $\boldsymbol{\beta}_{\mathbf{r}^{(k)}}^{(k)}$ while Yang et al. (2016) considered the g-prior (which significantly simplifies the calculation), some of our conditions are slightly more stringent.

- (1) The first condition is on the true regression coefficients $\boldsymbol{\beta}^{(k)*}$.

- (1a) For some $B_1 \geq 1$,

$$\frac{1}{n} \left\| \mathbf{X}^{(k)} \boldsymbol{\beta}^{(k)*} \right\|_2^2 \leq B_1 \sigma^2 \log p.$$

- (1b) For some $B_2 \geq 0$,

$$\frac{1}{n} \left\| \mathbf{X}_{(\mathbf{r}^{(k)*})^c}^{(k)} \boldsymbol{\beta}_{(\mathbf{r}^{(k)*})^c}^{(k)*} \right\|_2^2 \leq B_2 \sigma^2 \frac{\log p}{n}.$$

Condition (1a) requires that the order of the total signal level $\|\mathbf{X}^{(k)} \boldsymbol{\beta}^{(k)*}\|_2^2$ is at most $n \log p$, and Condition (1b) requires that noninfluential covariates cannot contribute significantly to the variation in $\mathbf{y}^{(k)}$. Both are reasonable assumptions for most high-dimensional problems. If one assumes all nonzero entries of $\boldsymbol{\beta}^{(k)*}$ are sufficiently large in absolute value, then $\boldsymbol{\beta}_{(\mathbf{r}^{(k)*})^c}^* = 0$ and Condition (1b) holds trivially. If one further assumes the influential covariates have bounded regression coefficients (i.e., coefficients do not grow with n), Condition (1a) allows each data set to have $O(\log p)$ independent influential covariates, which is not restrictive when $p \gg n$. More discussion on Condition (1a) will be given after Condition (5).

- (2) The second condition is on the design matrix. For any symmetric matrix \mathbf{A} , denote its smallest eigenvalue as $\lambda_{\min}(\mathbf{A})$.

- (2a) $\|\mathbf{X}_j^{(k)}\|_2^2 = n$ for all $j = 1, \dots, p$.

- (2b) For some $\nu \in (0, 1]$,

$$\min_{|\mathbf{r}| \leq L} \lambda_{\min} \left(\frac{1}{n} (\mathbf{X}_{\mathbf{r}}^{(k)})^T \mathbf{X}_{\mathbf{r}}^{(k)} \right) \geq \nu.$$

(2c) For some $B_3 \geq 8/\nu$, we have

$$\frac{1}{\sqrt{n}} \mathbb{E}_{\mathbf{Z}} \left[\max_{|\mathbf{r}| \leq L} \max_{\mathbf{s} \subseteq \mathbf{r}^c} |\mathbf{Z}^\top (\mathbf{I} - \boldsymbol{\Psi}_{\mathbf{r}}^{(k)}) \mathbf{X}_{\mathbf{s}}^{(k)}| \right] \leq \frac{1}{2} \sqrt{B_3 \nu \log p},$$

where $\mathbf{Z} \sim \mathcal{N}(\mathbf{0}, \mathbf{I})$ and $\boldsymbol{\Psi}_{\mathbf{r}}^{(k)} = \mathbf{X}_{\mathbf{r}}^{(k)} ((\mathbf{X}_{\mathbf{r}}^{(k)})^\top \mathbf{X}_{\mathbf{r}}^{(k)})^{-1} \mathbf{X}_{\mathbf{r}}^{(k)}$ is the projection matrix.

Condition (2a) assumes all columns of $\mathbf{X}^{(k)}$ are normalized and is used to simplify the calculation. Conditions (2b) and (2c) are known as lower restricted eigenvalue and sparse projection condition respectively (Yang et al., 2016). The former is a modest constraint that is necessary for theoretical analysis of Bayesian variable selection problems (Narisetty and He, 2014). The latter can always be satisfied by choosing some $B_3 = O(L)$; see Yang et al. (2016) for more discussion.

(3) The third condition is on the choice of prior hyperparameters. Let $\tilde{\sigma}_0^2 = \sigma_0^2/\sigma^2$, and C denote some universal constant (i.e., a constant that does not depend on n).

(3a) $1 + n\tilde{\sigma}_0^2 \leq Cp^{2\alpha}$ for some $\alpha > 0$.

(3b) $L \leq Cp^\beta$ for some $\beta \in (0, 1)$.

(3c) $\{\omega_k\}_{k=1}^K$ satisfies (8) and

$$\frac{\omega_k}{k} > \frac{3}{2} \left(\frac{B_1}{\nu\tilde{\sigma}_0^2} + B_2 + B_3 \right) + \beta + 2.$$

(3d) The function f in (7) satisfies

$$1 \leq \frac{f(k+1, L)}{f(k, L)} \leq L, \quad \forall k = 1, 2, \dots$$

In the high-dimensional setting with $n \ll p$, both Conditions (3a) and (3b) are very natural and easy to satisfy. Condition (3c) requires the parameter ω_k to be sufficiently large, which is needed to ensure that the posterior mass concentrates on sparse models. Condition (3d) implies that $f(|\gamma|, L) \leq L^{|\gamma|}$. By Conditions (3b) and (3c), the product term in (7) is not greater than $p^{-2|\gamma|}$, and thus the magnitude of $\Pi(\gamma)$ depends little on the function $f(|\gamma|, L)$.

(4) The true sparsity level $|\mathbf{r}^{(k)*}|$ satisfies

$$\max \left\{ 1, |\mathbf{r}^{(k)*}| \right\} \leq \frac{n}{25 \log p}.$$

(5) The constant $C_{\beta, k}$ satisfies

$$C_{\beta, k} = \left\{ 8 \left(\frac{\omega_k}{k} + 2 + \alpha \right) + \frac{12B_1}{\nu\tilde{\sigma}_0^2} \right\} \frac{\sigma^2 \log p}{n\nu}.$$

Condition (5) is known as the beta-min condition (Yang et al., 2016). By (8), it further implies that $C_{\beta, K} < C_{\beta, K-1} < \dots < C_{\beta, 1}$; that is, the more data sets in which the covariate is influential, the lower the signal strength level required to detect it. To gain further insights into this condition,

consider the ideal case where $\omega_k/k, \alpha, B_1, \nu, \tilde{\sigma}_0^2, \sigma^2$ are all universal constants. Then, as long as $\log p = o(n)$ (which is the asymptotic regime considered in most high-dimensional works), $C_{\beta,k}$ goes to zero implying that we can identify activated covariates with diminishing signal sizes. If all entries of $(\beta^{(k)*})^2$ corresponding to influential covariates only have order $n^{-1} \log p$, then we have $\|\mathbf{X}^{(k)} \beta^{(k)*}\|_2^2 = O(|\mathbf{r}^{(k)*}| \log p)$, which is much smaller than the order $n \log p$ required by Condition (1a).

Theorem 1. Suppose for each k , $\mathbf{y}^{(k)}$ is generated by (1) with $\beta^{(k)} = \beta^{(k)*}$. If Conditions (1) to (5) hold, we have

$$\mathbb{P} \left(\left\{ \Pi(\gamma^* | (\mathbf{y}^{(k)})_{k \in [K]}) \geq 1 - c_1 p^{-1} \right\} \right) \geq 1 - c_2 p^{-c_3},$$

where $\Pi(\cdot | (\mathbf{y}^{(k)})_{k \in [K]})$ denotes the posterior measure for the model specified by Equations (1) to (7), \mathbb{P} denotes the probability measure for the true data-generating process, and c_1, c_2 and c_3 are positive universal constants.

Proof. We defer the proof to Appendix A. □

2.3 Multi-task Sum of Single Effects Model

For Bayesian problems, posterior distributions are typically calculated through Markov Chain Monte Carlo (MCMC) sampling. But in our case, the huge discrete model space can make the sampling converge very slowly. In this section, we approximate our muSSVS model by a multi-task sum of single effects (muSuSiE) model, which is based on the recently developed “sum of single effects” model of Wang et al. (2020a) for a single variable selection problem. It enables us to propose an iterative Bayesian stepwise selection (IBSS) method which can quickly yield an approximate Bayesian solution to the multi-task variable selection problem. The muSuSiE model is given as follows:

$$\begin{aligned} \mathbf{y}^{(k)} &= \mathbf{X}^{(k)} \beta^{(k)} + \mathbf{e}^{(k)}, \text{ where } \mathbf{e}^{(k)} \sim \mathcal{N}_{n_k}(0, \sigma_{(k)}^2 \mathbf{I}_{n_k}), \\ \beta^{(k)} &= \sum_{l=1}^L \beta_l^{(k)}, \\ \beta_l^{(k)} &= \phi_l \times b_l^{(k)} \times \mathbf{r}_l^{(k)}, \text{ where } \mathbf{r}_l^{(k)} = \sum_{I \in \mathcal{I}_k} \gamma_l^I, \text{ and } \mathcal{I}_k \text{ is given by (6),} \\ (\phi_l)_{l \in [L]}, (\gamma_l)_{l \in [L]}, (b_l^{(k)})_{l \in [L], k \in [K]} &\text{ are independent, and} \\ \phi_l &\sim \text{Bernoulli}(\pi_\phi), \\ \gamma_l &= (\gamma_l^I)_{I \in \mathcal{P}_K} \sim \text{Multinomial}(1, \boldsymbol{\pi}), \\ b_l^{(k)} &\sim \mathcal{N}_1(0, \sigma_{0l(k)}^2). \end{aligned} \tag{9}$$

The vectors $\gamma_1, \dots, \gamma_L$ take value in $\{0, 1\}^{|\mathcal{P}_K|p}$, and each γ_l has exactly one non-zero entry since it follows a multinomial distribution with size parameter equal to 1. The choice of the hyperparameter $\boldsymbol{\pi} \in \mathbb{R}^{|\mathcal{P}_K|p}$ will be discussed shortly. In words, the above model encodes the following procedure for selecting activated variables. For $l = 1, \dots, L$:

1. Draw $\gamma_l \sim \text{Multinomial}(1, \pi)$. Then $(\gamma_l)_j^I = 1$ for some $j \in [p]$ and $I \in \mathcal{P}_K$, and we propose to activate covariate j in the data sets indexed by I .
2. Draw $\phi_l \sim \text{Bernoulli}(\pi_\phi)$. If $\phi_l = 1$, we “accept the proposal,” and for each $k \in I$, we set $\beta_j^{(k)} = b_l^{(k)}$ where $b_l^{(k)}$ is drawn independently from $\mathcal{N}_1(0, \sigma_{0l(k)}^2)$.

For each $k \in [K]$, $\mathbf{r}_l^{(k)} \in \{0, 1\}^p$ is a binary vector such that $|\mathbf{r}_l^{(k)}| = 1$ if the l -th proposed covariate is activated in the k -th data set (i.e., $\phi_l = 1$), and $|\mathbf{r}_l^{(k)}| = 0$ otherwise. We call each $\beta_l^{(k)}$ a “single-effect” vector. The vector of regression coefficients of the k -th data set, $\beta^{(k)} \in \mathbb{R}^p$, is defined as the summation of L single-effect vectors $\beta_1^{(k)}, \dots, \beta_L^{(k)}$, which explains why this model is called “sum of single effects.” The use of the Bernoulli random variables ϕ_1, \dots, ϕ_L guarantees that the number of truly activated covariates can range from 0 to L , which is one key difference between muSuSiE and the original SuSiE model of Wang et al. (2020a). Another way to think of this is that we decompose the variable selection model into the sum of L single-effect or null models.

For the hyperparameter π , we assume it is chosen such that if $\gamma \sim \text{Multinomial}(1, \pi)$, then for each $j \in [p]$ and $I \in \mathcal{P}_K$,

$$\gamma_j^I = 1 \text{ with probability } \pi_{|I|},$$

where $\pi_1 > \pi_2 > \dots > \pi_K > 0$ are some constants such that the vector π sums up to one. That is, we can write π as

$$\pi = \underbrace{(\pi_1, \dots, \pi_1)}_{\binom{K}{1}p}, \dots, \underbrace{(\pi_k, \dots, \pi_k)}_{\binom{K}{k}p}, \dots, \underbrace{(\pi_K, \dots, \pi_K)}_{\binom{K}{K}p} \in \mathbb{R}^{(2^K - 1)p}.$$

This choice of π means that with probability proportional to $\binom{K}{k}\pi_k$, we propose to activate some covariate in k data sets, and then the index of the covariate and the indices of the k data sets are chosen randomly with equal probability.

Let $\gamma = \sum_{l=1}^L \phi_l \gamma_l$. Note that γ may not take value in the model space \mathbb{M}_γ defined in (5), since the same covariate may be selected multiple times in the L independent draws from $\text{Multinomial}(1, \pi)$. This is the only difference between muSuSiE and the muSSVSmodel described in Section 2.1. Indeed, if $\gamma \in \mathbb{M}_\gamma$ (that is, no covariate is selected more than once in the L draws), one can show that under the muSuSiE model, its prior probability is given by

$$\Pi(\gamma) = f(|\gamma|, L) \prod_{l=1}^L \pi_\phi^{\phi_l} (1 - \pi_\phi)^{1 - \phi_l} \pi_{|I_l|}^{\phi_l}, \quad (10)$$

where $I_l \in \mathcal{P}_K$ is the set such that $|\gamma_l^{I_l}| = 1$ and

$$f(|\gamma|, L) = L \times (L - 1) \times \dots \times (L - |\gamma| + 1).$$

Note that f satisfies Condition (3d). A straightforward calculation shows that (10) and (7) are equivalent, as long as one chooses $\omega_1, \dots, \omega_K$ such that

$$\frac{\pi_\phi \pi_k}{1 - \pi_\phi} = p^{-\omega_k}, \quad (11)$$

for each $k \in [K]$. This shows why muSuSiE is an approximation to the muSSVS model. We will see in the next section that, by allowing a covariate to be selected multiple times in the L single-effect models (which happens with very small probability when p is large), we can devise an efficient VB method for approximating the posterior distribution of γ .

2.4 Iterative Bayesian Stepwise Selection for fitting muSuSiE

We propose an iterative Bayesian stepwise selection (IBSS) method for fitting the model given in (9) by generalizing the IBSS algorithm of Wang et al. (2020a). The starting point for our approach is the “multi-task single-effect regression” model (muSER), a multi-task regression model where at most one of the p explanatory variables has a non-zero regression coefficient. To simplify the calculation, we assume the variance components $\sigma_{(k)}^2$ and $\sigma_{0l(k)}^2$ are shared across all K data sets and thus drop the subscript (k) . Letting $L = 1$ in (9), we obtain the following muSER model for K data sets,

$$\begin{aligned} \mathbf{y}^{(k)} &= \mathbf{X}^{(k)} \boldsymbol{\beta}^{(k)} + \mathbf{e}^{(k)}, \text{ where } \mathbf{e}^{(k)} \sim \mathcal{N}_{n_k}(0, \sigma^2 \mathbf{I}_{n_k}), \\ \boldsymbol{\beta}^{(k)} &= b^{(k)} \times \phi \times \mathbf{r}^{(k)}, \text{ where } \mathbf{r}^{(k)} = \sum_{I \in \mathcal{I}_k} \gamma_I^I, \text{ and } \mathcal{I}_k \text{ is given by (6),} \\ \phi &\sim \text{Bernoulli}(\pi_\phi), \\ \boldsymbol{\gamma} &\sim \text{Multinomial}(1, \boldsymbol{\pi}), \\ b^{(k)} &\sim \mathcal{N}_1(0, \sigma_0^2). \end{aligned} \tag{12}$$

Since we only allow at most one covariate is activated in (12), the posterior distribution of $(\boldsymbol{\gamma}, 1 - \phi)$ given σ^2 and σ_0^2 can be quickly calculated, which is given by

$$(\boldsymbol{\gamma}, 1 - \phi) | (\mathbf{y}^{(k)})_{k \in [K]}, \sigma^2, \sigma_0^2 \sim \text{Multinomial}(1, (\boldsymbol{\alpha}, \alpha_0)), \tag{13}$$

where $\boldsymbol{\alpha}$ and α_0 are defined in Appendix B. Further, the posterior distribution of $\beta_i^{(k)}$ given $r_i^{(k)} = 1$ and $\phi = 1$ is given by

$$\beta_i^{(k)} | (\mathbf{y}^{(k)})_{k \in [K]}, \sigma^2, \sigma_0^2 \sim \mathcal{N}(\mu_{1i}^{(k)}, \sigma_{1i(k)}^2),$$

where we defer the explicit expressions for $\mu_{1i}^{(k)}$ and $\sigma_{1i(k)}^2$ to Appendix B. For ease of notation, we introduce a function, f_{muSER} , which returns the posterior distribution for $\boldsymbol{\beta}$ under the muSER model. Since this posterior distribution is determined only by the values of $\boldsymbol{\alpha}$, α_0 , $\boldsymbol{\mu}_1^{(k)} = (\mu_{11}^{(k)}, \dots, \mu_{1p}^{(k)})$ and $\boldsymbol{\sigma}_{1(k)}^2 = (\sigma_{11(k)}^2, \dots, \sigma_{1p(k)}^2)$ for $k = 1, \dots, K$, we define

$$f_{\text{muSER}}((\mathbf{y}^{(k)})_{k \in [K]}; \sigma^2, \sigma_0^2) := \left(\boldsymbol{\alpha}, \alpha_0, \left\{ \boldsymbol{\mu}_1^{(k)} \right\}_{k=1}^K, \left\{ \boldsymbol{\sigma}_{1(k)}^2 \right\}_{k=1}^K \right). \tag{14}$$

Observe that for the muSuSiE model, if $\{\boldsymbol{\beta}_{l'} : l' \in [L] \text{ and } l' \neq l\}$ is given, calculating the posterior distribution of $\boldsymbol{\beta}_l$ is very straightforward: one just needs to fit the muSER model by substituting the residual $\mathbf{y}^{(k)} - \mathbf{X}^{(k)} \sum_{l' \neq l} \boldsymbol{\beta}_{l'}^{(k)}$ for the response $\mathbf{y}^{(k)}$ for each k . This suggests an iterative strategy for fitting muSuSiE model, which we detail in Algorithm 1.

Using the notation in Algorithm 1, we can express the posterior mean of the regression coefficients for the k -th data set by

$$\widehat{\boldsymbol{\beta}}^{(k)} = \sum_{l=1}^L \widehat{\boldsymbol{\beta}}_l^{(k)}. \tag{15}$$

By an argument similar to that in Wang et al. (2020a), we can show that this IBSS algorithm coincides with the coordinate ascent variational inference algorithm (Blei et al., 2017) for maximizing the ELBO over a particular variational family for the muSuSiE model; see Appendix B, where we also explain how to choose the stopping criterion and estimate σ^2 and σ_0^2 empirically.

Algorithm 1 Iterative Bayesian stepwise selection for fitting muSuSiE

Require: data $\{\mathbf{X}^{(k)}\}_{k=1}^K, \{\mathbf{y}^{(k)}\}_{k=1}^K$; number of effects L

Require: a function f_{muSER} which is defined in (14).

initialize posterior means $\hat{\beta}_l^{(k)} = 0$ for $l = 1, \dots, L$ and $k = 1, \dots, K$

initialize σ^2 and $\{\sigma_{0l}^2\}_{l=1}^L$

if the stopping criterion is not satisfied **then**

for $l = 1, \dots, L$ **do**

for $k = 1, \dots, K$ **do**

$\tilde{\mathbf{y}}_l^{(k)} \leftarrow \mathbf{y}^{(k)} - \mathbf{X}^{(k)} \sum_{l' \neq l} \hat{\beta}_{l'}^{(k)}$

end for

 estimating σ_{0l}^2 by maximizing (30)

$\left(\alpha_l, \alpha_{0l}, \left\{ \mu_{1l}^{(k)} \right\}_{k=1}^K, \left\{ \sigma_{1l}^{(k)} \right\}_{k=1}^K \right) \leftarrow f_{\text{muSER}}(\tilde{\mathbf{y}}_l; \sigma^2, \sigma_{0l}^2).$

for $k = 1, \dots, K$ **do**

$\hat{\beta}_l^{(k)} \leftarrow \left(\sum_{I \in \mathcal{I}_k} \alpha_l^{(I)} \right) \odot \mu_{1l}^{(k)}$ (\odot denotes elementwise multiplication)

end for

end for

 estimating σ^2 by (36).

end if

return $\{\alpha_l\}_{l=1}^L, \{\alpha_{0l}\}_{l=1}^L, \{\mu_{1l}^{(k)}\}_{l \in [L], k \in [K]}, \{\sigma_{1l}^{(k)}\}_{l \in [L], k \in [K]}, \{\hat{\beta}_l^{(k)}\}_{l \in [L], k \in [K]}$

3 Simulation Studies for Bayesian Multi-task Variable Selection

We conduct simulation studies to illustrate the benefits of performing variable selection for multiple data sets simultaneously rather than independently. We generate data sets according to (1) using the same σ^2 for all K data sets. For the true model, we consider two types of activated covariates. For the first type, each covariate is activated in all K data sets. We denote the set of these covariates by S_c^* and let $s_1^* = |S_c^*|$. For the second type, each covariate is activated in only one data set. We choose some $s_2^* > 0$ and draw s_2^* covariates of the second type for each data set; denote the set of covariates that are only activated in the k -th data set by $S_{s(k)}^*$. The true model size is then given by $s^* = s_1^* + K s_2^*$, and $S_{(k)}^* = S_c^* \cup S_{s(k)}^*$ is the true set of activated covariates for the k -th data set. For each activated covariate, we sample its regression coefficient $\beta_i^{(k)}$ independently from the normal distribution $\mathcal{N}(0, 0.6^2)$. For the design matrix, we sample each entry of $\mathbf{X}^{(k)} \in \mathbb{R}^{n \times p}$ from the standard normal distribution. Finally, we generate the response data by drawing $\mathbf{y}^{(k)} \sim \mathcal{N}(\mathbf{X}^{(k)} \beta^{(k)}, \sigma^2 \mathbf{I})$.

After generating the data set $\{(\mathbf{X}^{(k)}, \mathbf{y}^{(k)})\}_{k=1}^K$, we run the IBSS algorithm to fit the muSuSiE model, which does variable selection simultaneously for K data sets. For comparison, we also fit the SuSiE model using the algorithm of Wang et al. (2020a) for each data set separately. We will refer to the former as the multi-task method and the latter as the single analysis method. When running simulations, we set $L = s^* + K$ for the multi-task method and $L = s_1^* + s_2^* + 1$ for the single analysis method. We have also tried other values of L and observed that as long as L is larger than the true number of activated covariates, its choice has negligible effect on the estimates. For the hyperparameter $\boldsymbol{\pi}$ in the muSuSiE model, we set it by (11), and thus it suffices to specify $\omega_1, \dots, \omega_K$. When $K = 2$, we use $p^{-\omega_1} = p^{-1.1}/2$ and $p^{-\omega_2} = p^{-1.25}$; when $K = 5$, we

p	n	s_1^*	s_2^*	sens_mu	sens_si	prec_mu	prec_si
600	100	10	2	0.4526	0.2632	0.9884	0.9365
600	100	10	5	0.3456	0.2045	0.9747	0.9258
1000	500	10	2	0.8121	0.7063	0.9962	1
1000	500	10	5	0.7905	0.7011	0.9928	0.9996
1000	500	25	2	0.8191	0.696	0.9985	1
1000	500	25	5	0.804	0.6949	0.9964	0.9999

Table 1: Simulation results for two data sets with $\sigma = 1$. For each setting, the result is averaged over 500 replicates.

use $\omega_1 = 1.4, \omega_2 = 1.55, \omega_3 = 1.7, \omega_4 = 1.85$ and $\omega_5 = 2$.

For the multi-task method, recall that for each l , the muSuSiE model returns the probability vector α_l defined in (13). Thus, the probability that the j -th coordinate is activated in the k -th data set in the l -th single-effect model is

$$\hat{r}_{lj}^{(k)} = \sum_{I \in \mathcal{I}_k} \alpha_{lj}^I,$$

where \mathcal{I}_k is given by (6). Taking all L single-effect vectors into account, we can calculate the probability that the j -th covariate is activated in the k -th data set by

$$\hat{r}_j^{(k)} = 1 - \prod_{l=1}^L (1 - \hat{r}_{lj}^{(k)}).$$

Setting the threshold to 0.5, we define the selected activated covariates from our multi-task method by

$$S_{\text{mu}(k)} = \{j : \hat{r}_j^{(k)} \geq 0.5\},$$

where “mu” indicates the multi-task method. For the standard SuSiE method, we use the `susie` function from the `susier` package (Wang et al., 2020a) to find the set of activated covariates, which we denote by $S_{\text{si}(k)}$; “si” in the subscript indicates the single analysis method. To compare the performance of two approaches, we calculate the sensitivity (sens) and precision (prec) by

$$\text{sens}(S_{(k)}) = \frac{|S_{(k)} \cap S_{(k)}^*|}{|S_{(k)}^*|}, \quad \text{prec}(S_{(k)}) = \frac{|S_{(k)} \cap S_{(k)}^*|}{|S_{(k)}|},$$

where we let $S_{(k)} = S_{\text{mu}(k)}$ for the multi-task method and $S_{(k)} = S_{\text{si}(k)}$ for the single analysis method.

Table 1 shows the simulation results for $\sigma^2 = 1$ and $K = 2$. We consider two scenarios: one with $p = 600$ and $n = 100$, and another with $p = 1000$ and $n = 500$. From Table 1, we observe that when the sample size is small ($n = 100$), the multi-task method will identify more activated covariates than the single analysis method, resulting in higher sensitivity and precision. When the sample size is increased to 500, the multi-task method still improves the sensitivity but slightly reduces the precision, because the multi-task method tends to treat the covariates with a very strong signal strength in only one data set as simultaneously activated in two data sets. Nevertheless, considering the significant improvement in sensitivity, the performance of the multi-task method is still much

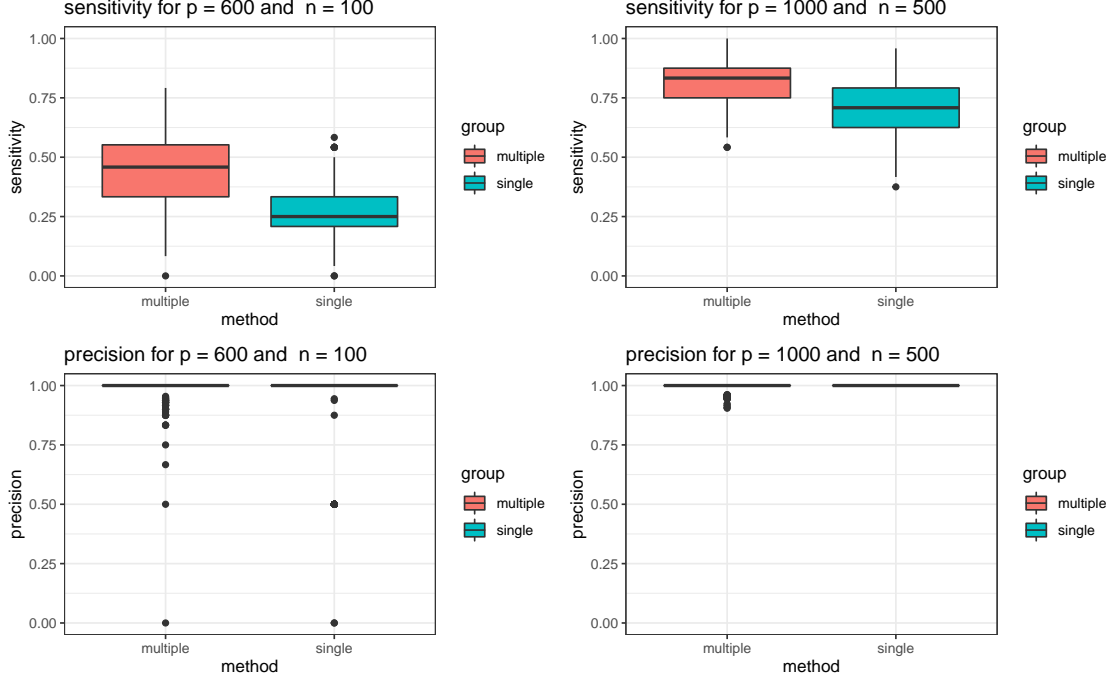


Figure 1: Sensitivity and precision for the simulation study with $K = 2$. Each box shows the distribution of sensitivity or precision among 500 replicates.

p	n	s_1^*	s_2^*	sens_mu	sens_si	prec_mu	prec_si
600	100	10	2	0.5976	0.2551	0.9907	0.9328
600	100	10	5	0.495	0.2007	0.9795	0.9269
1000	500	10	2	0.8181	0.7062	0.9936	0.9999
1000	500	10	5	0.7921	0.7025	0.9887	0.9998
1000	500	25	2	0.8261	0.6927	0.9974	0.9999
1000	500	25	5	0.8101	0.6916	0.9938	0.9999

Table 2: Simulation results for five data sets with $\sigma = 1$. For each setting, the result is averaged over 500 replicates.

better. To further examine this phenomenon, we plot the sensitivity and specificity for $|s_1^*| = 10$ and $|s_2^*| = 2$ in Figure 1; all other settings yield similar plots.

The simulation results for $\sigma^2 = 1$ and $K = 5$ are shown in Table 2. It is worth noting that when the sample size is small, compared with the simulation study with $K = 2$, the advantage of the multi-task method on five data sets becomes much more significant and it outperforms the single analysis method significantly in terms of both sensitivity and precision. When the sample size is large, the multi-task method is still better than the single analysis method, but the performance is similar to that for $K = 2$. The simulation results for $\sigma^2 = 4$ (which represents a higher noise level) are shown in Appendix C, where we have made very similar observations for the behavior of the two methods.

4 Differential DAGs Analysis via Multi-task Variable Selection

4.1 From Multi-task Variable Selection to Joint Estimation of Multiple DAG models

A highly useful application of the proposed Bayesian multi-task variable selection method is that it can be naturally extended to the multi-task structure learning problem, i.e., joint estimation of multiple DAG models. The existing Bayesian literature on the statistical learning of multiple graphs mostly focuses on undirected graphical models; see, for example, [Danaher et al. \(2014\)](#); [Peterson et al. \(2015\)](#); [Gonçalves et al. \(2016\)](#); [Niu et al. \(2018\)](#); [Peterson et al. \(2020\)](#); [Shaddox et al. \(2020\)](#); [Peterson and Stingo \(2021\)](#). For DAG models, [Oyen and Lane \(2012\)](#) proposed a greedy search algorithm on the DAG space, and [Yajima et al. \(2015\)](#) devised an MCMC sampler which extends the method of [Fronk and Giudici \(2004\)](#) and uses single-edge additions, deletions and reversals to explore the DAG space. For frequentists' approaches, the recent work of [Chen et al. \(2021\)](#) proposed an iterative constrained optimization algorithm for calculating an ℓ^1/ℓ^2 -regularized maximum likelihood estimator, [Wang et al. \(2020b\)](#) extended the well-known greedy equivalence search (GES) algorithm of [Chickering \(2002\)](#) to the case of multiple DAGs, and [Ghoshal et al. \(2019\)](#) offered an algorithm that learns the difference between the DAGs efficiently but seems only applicable to the case $K = 2$. The method we will propose in this section is motivated by the observation that once the order of variables is given, the IBSS algorithm for multi-task variable selection can be applied to quickly learn multiple DAG models simultaneously. Hence, all we need is just to combine IBSS with an MCMC sampler that traverses the order space. Compared with frequentists' methods, our algorithm can quantify the learning uncertainty since the estimators are averaged over the posterior distribution.

Consider learning the DAG model for a single data set first. Let $\mathcal{G} = (V, E)$ be a directed acyclic graph with vertices $V = \{1, \dots, p\}$ and set of directed edges $E \subset V \times V$. Let $|\mathcal{G}|$ denote the cardinality of the edge set E . Let $\mathbf{B} \in \mathbb{R}^{p \times p}$ be the weighted adjacency matrix of the DAG \mathcal{G} such that $B_{ij} \neq 0$ if and only if $(i, j) \in E$. Suppose that the observed data matrix, denoted by $\mathbf{X} \in \mathbb{R}^{n \times p}$, is generated by the following linear structural equation model (SEM),

$$\mathbf{X}_j = \sum_{i=1}^p B_{ij} \mathbf{X}_i + \mathbf{e}_j, \quad \text{for } j = 1, \dots, p. \quad (16)$$

where \mathbf{X}_j denotes the j -th column of \mathbf{X} , and for each j , the error vector \mathbf{e}_j independently follows $\mathcal{N}_n(0, \sigma_j^2 \mathbf{I})$. That is, each row of \mathbf{X} can be seen as an i.i.d. copy of a random vector $\mathbf{X} = (X_1, \dots, X_p)$, whose distribution is given by

$$\mathbf{X} = \mathbf{B}^T \mathbf{X} + \mathbf{e}, \quad \mathbf{e} \sim \mathcal{N}_p(0, \text{diag}(\sigma_1^2, \dots, \sigma_p^2)).$$

Since \mathcal{G} is acyclic, there exists at least one permutation (i.e., order) $\prec \in \mathbb{S}_p$ such that B_{ij} equals 0 for any $j \prec i$ (i.e., j precedes i in the permutation \prec), where \mathbb{S}_p is the symmetric group of order p . Hence, if the rows and columns of \mathbf{B} are permuted according to \prec , the resulting matrix is strictly upper triangular. To determine which entries in \mathbf{B} are not zero, we can convert this problem to p variable selection problems. If we know that the DAG is consistent with the order \prec , for each j , we only need to identify the parent nodes for j from the set $\{i \in [p]: i \prec j\}$, which can be seen as a variable selection problem with response variable X_j and candidate explanatory variables $\{X_i: i \prec j\}$. Combining the results for all p variable selection problems, we get an estimate for

the DAG model underlying the distribution of \mathbf{X} . Unfortunately, the true order of nodes is usually unknown in practice and needs to be learned from the data. Since the order space \mathbb{S}^p has cardinality $p!$, searching over \mathbb{S}^p can be very time consuming, which is one major challenge in structure learning. To overcome this, various order MCMC methods have been proposed in the literature for efficiently generating samples from posterior distributions defined on \mathbb{S}^p (Koller and Friedman, 2009; Kuipers and Moffa, 2017; Agrawal et al., 2018; Kuipers et al., 2022).

Next, consider the joint learning of multiple DAG models from K data sets, one for each data set. This problem, which henceforth is referred to as differential DAG analysis, is motivated by differential gene regulatory network (GRN) analysis in biology, where we may have gene data for samples from different tissues, developmental phases or case-control studies and the goal is to see how the GRN changes across different samples (Li et al., 2020). Since the advent of the single-cell technology, differential GRN analysis has become increasingly important (Fiers et al., 2018; Van de Sande et al., 2020). As in the multi-task variable selection problem, we assume the same p covariates are observed in K data sets, and use $\mathbf{X}^{(k)} \in \mathbb{R}^{n_k \times p}$ to denote the data matrix for the k -th data set with sample size n_k . Denote the K DAGs we want to learn by $\{\mathcal{G}^{(k)} = (V, E^{(k)})\}_{k=1}^K$, which share the same node set $V = [p]$ and, a priori, are believed to share a large proportion of common edges. We further assume that $\mathcal{G}^{(1)}, \dots, \mathcal{G}^{(K)}$ are “permutation compatible,” which means that for any $i \neq j$, if $(i, j) \in E^{(k)}$ for some $k \in [K]$, then $(j, i) \notin E^{(k')}$ for any $k' \in [K]$. In other words, we assume there exists a order shared by all the K DAGs. This is a very reasonable assumption to make for problems such as GRN analysis, where an edge may occur only in some data sets but generally does not change direction. Observe that if the order \prec is known, learning K DAGs can be converted to p multi-task variable selection problems. One just needs to repeatedly apply the IBSS algorithm we have proposed to select the parent nodes for each $j \in [p]$. Denote the resulting K DAGs by $\{\mathcal{G}_{\prec}^{(k)}\}_{k=1}^K$. We are interested in the case where the ordering is unknown. To average over the order space, we follow the existing order MCMC works to devise a Metropolis-Hastings algorithm on \mathbb{S}^p , which we describe in detail in the next subsection.

4.2 An Order MCMC Sampler for Differential DAG Analysis

We propose to consider the following Gibbs posterior distribution (Jiang and Tanner, 2008),

$$P(\prec | \{\mathbf{X}^{(k)}\}_{k=1}^K) \propto P(\{\mathcal{G}_{\prec}^{(k)}\}_{k=1}^K | \prec) \prod_{k=1}^K \hat{P}(\mathbf{X}^{(k)} | \mathcal{G}_{\prec}^{(k)}), \quad \forall \prec \in \mathbb{S}^p, \quad (17)$$

where $\{\mathcal{G}_{\prec}^{(k)}\}_{k=1}^K$ denotes the DAGs we obtain by applying the IBSS algorithm with ordering \prec . The product term in (17) denotes the “estimated” likelihood function, which gives the estimated probability of observing the data given that $\mathcal{G}_{\prec}^{(k)}$ is the underlying DAG model for the k -th data set. Recall that when fitting the muSuSiE model for multi-task variable selection, the IBSS algorithm yields estimates $\hat{\beta}^{(1)}, \dots, \hat{\beta}^{(K)}$ and $\hat{\sigma}^2$, where $\hat{\beta}^{(k)}$ is the estimated posterior mean of the vector of regression coefficients for the k -th data set and $\hat{\sigma}^2$ is the estimated error variance; see Equations (15) and (36). Denote by $\mathcal{A}_j^{\prec} = \{i \in [p] : i \prec j\}$ the index set of variables preceding \mathbf{X}_j in the order \prec . For the variable selection problem with response vector \mathbf{X}_j and covariates $\{\mathbf{X}_i : i \in \mathcal{A}_j^{\prec}\}$, let $\hat{\beta}_{j,\prec}^{(k)}$ be the estimated regression coefficients and $\hat{\sigma}_{j,\prec}^2$ be the estimated error variance from IBSS. Then, we can estimate the likelihood of the DAGs $\{\mathcal{G}_{\prec}^{(k)}\}_{k=1}^K$ by plugging in the estimates $\{\hat{\beta}_{j,\prec}^{(k)}\}_{k \in [K], j \in [p]}$

and $\{\hat{\sigma}_{j,\prec}^2\}_{j \in [p]}$, which yields

$$\prod_{k=1}^K \hat{P}(\mathbf{X}^{(k)} | \mathcal{G}_{\prec}^{(k)}) = \prod_{k=1}^K \prod_{j=1}^p \prod_{i=1}^{n_k} \Phi \left(\frac{X_{ij}^{(k)} - \mathbf{X}_{i, \mathcal{A}_j^{\prec}}^{(k)} \hat{\boldsymbol{\beta}}_{j,\prec}^{(k)}}{\hat{\sigma}_{j,\prec}} \right), \quad (18)$$

where $\Phi(x)$ is the density function for the standard normal distribution and $\mathbf{X}_{i, \mathcal{A}_j^{\prec}}^{(k)}$ denotes the row vector with entries $\{\mathbf{X}_{il}^{(k)} : l \in \mathcal{A}_j^{\prec}\}$. The first term $P(\{\mathcal{G}_{\prec}^{(k)}\}_{k=1}^K | \prec)$ in (17) is the prior probability of the DAGs $\{\mathcal{G}_{\prec}^{(k)}\}_{k=1}^K$ given order \prec , or more generally can be any positive function that penalizes DAGs with more edges. Recall the probability vector $\boldsymbol{\alpha}$ defined in (13), which gives the estimated posterior probability of an entry of the indicator vector $\boldsymbol{\gamma}$ being equal to one. Let $\boldsymbol{\alpha}_{i,\prec}$ be the probability vector for the variable selection problem with response vector \mathbf{X}_j and covariates $\{\mathbf{X}_i : i \in \mathcal{A}_j^{\prec}\}$. We define the penalty by

$$P(\{\mathcal{G}_{\prec}^{(k)}\}_{k=1}^K | \prec) = \prod_{k=1}^K \prod_{j=1}^p p^{-\omega_k \sum_{I \in \mathcal{P}_K, |I|=k} |\boldsymbol{\alpha}_{j,\prec}^I|}, \quad (19)$$

where $|\boldsymbol{\alpha}_{j,\prec}^I|$ denotes the ℓ^1 -norm of the vector $\boldsymbol{\alpha}_{j,\prec}^I$ and we recall $\omega_1, \dots, \omega_K$ are the hyperparameters introduced in (7) for muSSVS and can be seen as a reparameterization of $\boldsymbol{\pi}$ by (11). The reasoning behind (19) is the same as that behind (7): observe that for each $k \in [K]$, the sum $\sum_{j \in [p]} \sum_{I \in \mathcal{P}_K, |I|=k} |\boldsymbol{\alpha}_{j,\prec}^I|$ gives the expected number of edges that are activated in k different data sets. Combining (18) and (19), we get a closed-form expression for the posterior defined in (17). For later use, let $\mathbf{R}_{\prec}^{(k)} \in [0, 1]^{p \times p}$ be the matrix such that the j -th column of $\mathbf{R}_{\prec}^{(k)}$ is given by

$$(\mathbf{R}_{\prec}^{(k)})_j = \sum_{I \in \mathcal{I}_k} \boldsymbol{\alpha}_{j,\prec}^I, \quad (20)$$

where we recall the definition of \mathcal{I}_k given in (6). That is, $(\mathbf{R}_{\prec}^{(k)})_{ij}$ is the estimated probability of the edge (i, j) in the k -th data set given the order \prec .

Given the target posterior distribution defined in (17), we are now ready to introduce our Metropolis-Hastings algorithm for differential DAG analysis. Given the current state $\prec \in S_p$, we propose another state \prec' from some proposal distribution $q(\cdot | \prec)$ and accept it with probability

$$\min \left\{ 1, \frac{P(\prec' | \{\mathbf{X}^{(k)}\}_{k=1}^K) q(\prec | \prec')}{P(\prec | \{\mathbf{X}^{(k)}\}_{k=1}^K) q(\prec' | \prec)} \right\}. \quad (21)$$

We choose $q(\cdot | \prec)$ to be the uniform distribution on the set of permutations that can be obtained from \prec by an adjacent transposition. That is, we randomly pick $j \in [p-1]$ with equal probability and then propose to move from $\prec = (i_1, \dots, i_j, i_{j+1}, \dots, i_p)$ to $\prec' = (i_1, \dots, i_{j+1}, i_j, \dots, i_p)$. Clearly, $q(\prec | \prec') = q(\prec' | \prec)$, and thus the proposal ratio in (21) is always equal to 1. Note that to calculate $P(\prec' | \{\mathbf{X}^{(k)}\}_{k=1}^K)$, we need to run IBSS to find the DAGs $\{\mathcal{G}_{\prec}^{(k)}\}_{k=1}^K$. Running this Metropolis-Hastings sampler for T iterations (excluding burn-in), we obtain a sequence of permutations denoted by $\{\prec_t\}_{t=1}^T$. For each \prec_t , let $\mathbf{R}_{\prec_t}^{(k)} \in [0, 1]^{p \times p}$ be the matrix defined in (20), and then $\{\mathbf{R}_{\prec_t}^{(k)}\}_{t=1}^T$ can

be used for making posterior inference. For example, to estimate the probability of the edge $i \rightarrow j$ being in the k -th DAG model, we can simply calculate the time average

$$\hat{R}_{ij}^{(k)} := \frac{1}{T} \sum_{t=1}^T (\mathbf{R}_{\prec_t}^{(k)})_{ij}. \quad (22)$$

5 Simulation Studies for Bayesian Differential DAG Analysis

We use simulation studies to investigate the performance of the order MCMC sampler described in Section 4.2, which we denote by muSuSiE-DAG, in two scenarios: $K = 2, n_1 = n_2 = 300$, and $K = 5, n_1 = \dots = n_5 = 240$. We fix the number of nodes p to 100 for all experiments. For each experiment, we generate the data according to the linear SEM (16) with true order given by $\prec = (1, 2, \dots, p)$. Hence, the true weighted adjacency matrices of the K DAGs are strictly upper triangular. The true DAGs $\{\mathcal{G}^{(k)}\}_{k=1}^K$ are then generated as follows. First, we generate a random edge set \mathcal{E}_{com} consistent with \prec such that each edge in \mathcal{E}_{com} is activated in all the K data sets. Second, for each $k \in [K]$, we generate an edge set $\mathcal{E}_{\text{pri}}^{(k)}$ which consists of edges that are only activated in the k -th data set. Let $N_{\text{com}} = |\mathcal{E}_{\text{com}}|$ denote the number of edges shared by all the K DAGs and $N_{\text{pri}} = |\mathcal{E}_{\text{pri}}^{(k)}|$ denote the number of “private” edges unique to each data set. We consider $N_{\text{com}} \in \{50, 100\}$, and $N_{\text{pri}} \in \{20, 50\}$ in the simulation studies. To generate the matrix $\mathbf{B}^{(k)}$ corresponding to DAG $\mathcal{G}^{(k)}$ and the error variances of the p variables, we follow Wang et al. (2020b) to sample the nonzero entries of $\mathbf{B}^{(k)}$ (determined by $\mathcal{G}^{(k)}$) independently from the uniform distribution on $[-1, -0.1] \cup [0.1, 1]$ and sample the error variance of each variable independently from the uniform distribution on $[1, 2.25]$. Note that for each edge in \mathcal{E}_{com} , its weights in the K data sets are drawn independently.

For each simulation setting, we generate 50 replicates; the true DAG models and the data $\{\mathbf{X}^{(k)}\}_{k=1}^K$ are re-sampled for each replicate. We compare the performance of four methods: PC algorithm or GES applied independently to each data set (Spirtes et al., 2000; Harris and Drton, 2013; Chickering, 2002), our muSuSiE-DAG method, and the joint GES algorithm proposed by Wang et al. (2020b) which is a state-of-the-art method for joint learning multiple DAG models with theoretical guarantees. We implement the PC and GES algorithms using the R package `pcalg` (Kalisch et al., 2012). For all four methods, we choose the parameter values that appear to have the best empirical performance in our experiments. For the PC algorithm, we choose $\alpha = 0.005$, where α is the significance level used in the conditional independent tests, and for GES and joint GES methods, we let $\lambda = 2$, where λ is the l_0 -penalization parameter (scaled by $\log p$). For the muSuSiE-DAG method, we need to set the penalty parameters $\omega_1, \dots, \omega_K$. For $K = 2$, we use $p^{-\omega_1} = p^{-2}/2$ and $p^{-\omega_2} = p^{-2.25}$, and the choice for $K = 5$ is given in Appendix D. The results for all four methods obtained by using other parameter values are also provided in Appendix D.

Table 3 shows the results for $K = 2$, and the results for $K = 5$ are given in Appendix D. For each method, we calculate the average number of incorrect edges, denoted by N_{wrong} , the average true positive rate (TP) and the average false positive (FP) rate by ignoring the edge directions. As expected, joint GES and muSuSiE-DAG have significantly larger true positive rates than PC and GES methods, since the former two methods are able to utilize information from all the K data sets to infer common edges, which is particularly useful when an edge has a relatively small signal size in both data sets. Meanwhile, the two joint methods tend to have slightly larger false positive rates as well, since an edge with a very large signal size in one data set is likely to be identified by

method	K	N_{com}	N_{pri}	N_{wrong}	TP	FP
PC	2	100	20	28.29	0.7822	4e-04
GES	2	100	20	19.67	0.8482	3e-04
joint GES	2	100	20	15.5	0.9117	0.001
muSuSiE-DAG	2	100	20	12.95	0.9139	4e-04
PC	2	100	50	39.37	0.7475	3e-04
GES	2	100	50	24.84	0.8505	6e-4
joint GES	2	100	50	24.94	0.9003	0.0021
muSuSiE-DAG	2	100	50	18.93	0.8988	8e-04
PC	2	50	50	21.9	0.8121	6e-04
GES	2	50	50	15.74	0.8514	2e-04
joint GES	2	50	50	23.11	0.8836	0.0023
muSuSiE-DAG	2	50	50	15.05	0.877	6e-04

Table 3: Simulation results for joint estimation of multiple DAG models with $K = 2$. For each setting, the result is averaged over 50 replicates.

the joint method as existing concurrently in both data sets. However, note that the false positive rate of muSuSiE-DAG is still comparable to that of PC and GES and is much smaller than that of joint GES. Overall, muSuSiE-DAG has the best performance among all the four methods in all settings, and its advantage is more significant when the ratio $N_{\text{com}}/N_{\text{pri}}$ is larger.

6 A Real Data Example for Differential DAG Analysis

To evaluate the performance of the proposed muSuSiE-DAG method in real data analysis, we consider a pre-processed gene expression microarray data set used in Wang et al. (2020b), which consists of two groups of patients with ovarian cancer. The first group has 83 patients who have enhanced expression of stromal genes that are associated with a lower survival rate. The second group has 168 patients who have ovarian cancer of other subtypes. For both groups, we observe the expression levels of $p = 76$ genes which, according to the KEGG database (Kanehisa et al., 2012), participate in the apoptotic pathway. For more details about the original data set, see Tothill et al. (2008). Let \mathcal{G}_1 denote the underlying DAG model for the first group and \mathcal{G}_2 denote that for the second. The objective of this real data analysis is to detect the differences between the two DAGs $\mathcal{G}_1, \mathcal{G}_2$, which may be associated with the survival rate. As in Section 5, we compare the performance of four methods: PC, GES, joint GES and muSuSiE-DAG. Table 4 lists the number of edges detected by each method. The results for all four methods obtained by using other parameter values are provided in Appendix E, where one can also find results obtained by combining PC, GES and joint GES with stability selection (Meinshausen and Bühlmann, 2010). The results clearly illustrate the differences between the four methods. First, the percentage of shared edges in the two estimated DAGs (i.e., the “ratio” column in Table 4) is much larger for the two joint methods, which is consistent with both our theory and simulation results. For PC and GES, this ratio is always less than 0.3 in all parameter settings we have tried; see Tables 14 and 15 in Appendix E. This shows that when the sample size is not large, applying a structure learning method to two data sets separately is very likely to miss some gene-gene interactions existing in both gene regulatory networks. Second, joint GES has the largest shared ratio, and it is often much larger than that of

Method	Parameters	$ \mathcal{G}_1 $	$ \mathcal{G}_2 $	$ \mathcal{G}_1 \cap \mathcal{G}_2 $	N_{total}	ratio
PC	$\alpha = 0.005$	33	60	18	75	0.24
GES	$\lambda = 2$	99	148	43	204	0.2108
joint GES	$\lambda = 2$	64	68	59	73	0.8082
muSuSiE-DAG	$p^{-\omega_1} = p^{-1.5}/2, p^{-\omega_2} = p^{-2}$	42	92	41	93	0.4409

Table 4: Results for the real data analysis. $|\mathcal{G}_k|$: number of edges in the estimated DAG for the k -th group; $|\mathcal{G}_1 \cap \mathcal{G}_2|$: number of edges shared by both DAGs; N_{total} : total number of edges in two DAGs; ratio: the ratio of $|\mathcal{G}_1 \cap \mathcal{G}_2|$ to N_{total} .

muSuSiE-DAG. This is probably because joint GES is a two-step procedure where the first step is to learn a large DAG G^{union} , and in the second step G_1 and G_2 are constructed separately under the constraint that they must be sub-DAGs of G^{union} . If an edge only exists in one DAG or it exists in both but has very different regression coefficients in the two SEMs, it is not very likely to be included in G^{union} and thus cannot be detected in the second step of joint GES. Indeed, since $p = 76$ is relatively large and $n_1 = 83$ and $n_2 = 168$, we expect that more edges (especially those with small signal sizes) can be detected in G_2 than in G_1 , which is observed for PC, GES and muSuSiE-DAG.

7 Concluding Remarks

In this paper, we study the Bayesian multi-task variable selection problem and prove a high-dimensional strong selection consistency result for the multi-task spike-and-slab variable selection (muSSVS) model we propose. By extending the SuSiE model of Wang et al. (2020a) to multiple data sets, we show that muSSVS can be approximated by a model we call muSuSiE, which further enables us to propose a variational Bayes algorithm, IBSS, for efficiently approximating the posterior distribution of muSSVS. Simulation results show that, compared with performing variable selection separately for multiple data sets, the proposed method can achieve a significantly larger sensitivity at the cost of a slightly decreased precision. Next, we consider the problem of learning multiple DAG models. Observing that given the order of the variables, we can quickly learn multiple DAGs simultaneously using IBSS, we propose an efficient order MCMC sampler targeting a Gibbs posterior distribution on the order space. Both simulation results and real data analysis show that the proposed algorithm is able to identify substantially more edges shared across the data sets while still controlling the false positive rate.

This work also opens up some interesting problems for future research. First, we build the strong selection consistency for the muSSVS model while the variational algorithm we propose is based on the muSuSiE model. It would be interesting to investigate whether we can establish high-dimensional consistency results directly for the SuSiE or muSuSiE model under some mild conditions, which would serve as a more powerful theoretical guarantee for variational Bayesian model selection. Second, one can extend the posterior consistency results for the muSSVS model to multi-task structure learning, but this probably requires assuming some restrictive conditions such as strong faithfulness (Nandy et al., 2018). Last, note that the proposed algorithm for learning multiple DAGs can be seen as a combination of the IBSS algorithm and a vanilla Metropolis-Hastings algorithm on the order space. Hence, more advanced MCMC sampling techniques (e.g. parallel tempering) can be used to further accelerate the mixing of the sampler.

Acknowledgements

We thank Yuhao Wang for sharing with us the code for the joint GES method and the pre-processed real data set.

Appendices

A Proof of Posterior Consistency for Bayesian Multi-task Variable Selection

By (1) and (2), we find the marginal likelihood for a model \mathbf{r} after integrating out $(\boldsymbol{\beta}^{(k)})_{k \in [K]}$ is

$$P((\mathbf{y}^{(k)})_{k \in [K]} | \mathbf{r}) \propto \prod_{k=1}^K \left| \boldsymbol{\Sigma}_{0(k)}^{-1} \right|^{1/2} \left| \frac{(\mathbf{X}_{\mathbf{r}^{(k)}}^{(k)})^T \mathbf{X}_{\mathbf{r}^{(k)}}^{(k)}}{\sigma^2} + \boldsymbol{\Sigma}_{0(k)}^{-1} \right|^{-1/2} \\ \times \exp \left\{ -\frac{1}{2\sigma^2} \left[(\mathbf{y}^{(k)})^T \left(\mathbf{I}_n - \mathbf{X}_{\mathbf{r}^{(k)}}^{(k)} \left((\mathbf{X}_{\mathbf{r}^{(k)}}^{(k)})^T \mathbf{X}_{\mathbf{r}^{(k)}}^{(k)} + \sigma^2 \boldsymbol{\Sigma}_{0(k)}^{-1} \right)^{-1} (\mathbf{X}_{\mathbf{r}^{(k)}}^{(k)})^T \right) \mathbf{y}^{(k)} \right] \right\}.$$

Denote

$$R_{\mathbf{r}^{(k)}}^{(k)} = (\mathbf{y}^{(k)})^T \left(\mathbf{I}_n - \mathbf{X}_{\mathbf{r}^{(k)}}^{(k)} \left((\mathbf{X}_{\mathbf{r}^{(k)}}^{(k)})^T \mathbf{X}_{\mathbf{r}^{(k)}}^{(k)} + \sigma^2 \boldsymbol{\Sigma}_{0(k)}^{-1} \right)^{-1} (\mathbf{X}_{\mathbf{r}^{(k)}}^{(k)})^T \right) \mathbf{y}^{(k)}, \\ R_{\mathbf{r}^{(k)}}^{(k)*} = (\mathbf{y}^{(k)})^T \left(\mathbf{I} - \mathbf{X}_{\mathbf{r}^{(k)}}^{(k)} ((\mathbf{X}_{\mathbf{r}^{(k)}}^{(k)})^T \mathbf{X}_{\mathbf{r}^{(k)}}^{(k)})^{-1} (\mathbf{X}_{\mathbf{r}^{(k)}}^{(k)})^T \right) \mathbf{y}^{(k)} = (\mathbf{y}^{(k)})^T (\mathbf{I}_n - \boldsymbol{\Psi}_{\mathbf{r}^{(k)}}^{(k)}) \mathbf{y}^{(k)}.$$

To simplify the notation, from now on we will omit superscript (k) whenever the statement applies to all $k = 1, \dots, K$. For example, when we write $R_{\mathbf{r}}$, it means $R_{\mathbf{r}^{(k)}}^{(k)}$ for any k . (The notation \mathbf{r} is abused here, since it may also refer to the complete model $\mathbf{r} = (\mathbf{r}^{(k)})_{k=1}^K$, but its meaning should be clear from context.) It is easy to check that we always have $R_{\mathbf{r}}^* \leq R_{\mathbf{r}}$. Indeed, let $\mathbf{X}_{\mathbf{r}} = \mathbf{U}_{n \times |\mathbf{r}|} \boldsymbol{\Lambda}_{|\mathbf{r}| \times |\mathbf{r}|} \mathbf{V}_{|\mathbf{r}| \times |\mathbf{r}|}^T$ be the singular value decomposition of $\mathbf{X}_{\mathbf{r}}$, then

$$R_{\mathbf{r}}^* = \|\mathbf{y}\|_2^2 - \mathbf{y}^T \mathbf{U} \mathbf{U}^T \mathbf{y}, \\ R_{\mathbf{r}} = \|\mathbf{y}\|_2^2 - \mathbf{y}^T \mathbf{U} \boldsymbol{\Lambda} (\boldsymbol{\Lambda}^2 + \sigma^2 \boldsymbol{\Sigma}_0^{-1})^{-1} \boldsymbol{\Lambda} \mathbf{U}^T \mathbf{y}.$$

Observe that $\boldsymbol{\Lambda} (\boldsymbol{\Lambda}^2 + \sigma^2 \boldsymbol{\Sigma}_0^{-1})^{-1} \boldsymbol{\Lambda}$ is a diagonal matrix with all diagonal entries being in $[0, 1]$. Hence, $R_{\mathbf{r}}^* \leq R_{\mathbf{r}}$. Let $D_{\mathbf{r}}$ denote the determinant term,

$$D_{\mathbf{r}} = |\boldsymbol{\Sigma}_0^{-1}|^{1/2} \left| \frac{\mathbf{X}_{\mathbf{r}}^T \mathbf{X}_{\mathbf{r}}}{\sigma^2} + \boldsymbol{\Sigma}_0^{-1} \right|^{-1/2} = |\mathbf{I}_{|\mathbf{r}|} + \tilde{\sigma}_0^2 \mathbf{X}_{\mathbf{r}}^T \mathbf{X}_{\mathbf{r}}|^{-1/2},$$

where the second equation follows from our assumption that all $\sigma_{0l(k)}^2$ are equal to σ_0^2 and $\tilde{\sigma}_0^2 = \sigma_0^2 / \sigma^2$. Using (7), we find that the posterior probability of \mathbf{r} is

$$\Pi(\mathbf{r} | (\mathbf{y}^{(k)})_{k \in [K]}) \propto \mathbb{1}\{\boldsymbol{\gamma} \in \mathbb{M}_{\boldsymbol{\gamma}}\} f(|\boldsymbol{\gamma}|, L) \prod_{k=1}^K \left\{ D_{\mathbf{r}^{(k)}} \exp \left(-\frac{R_{\mathbf{r}^{(k)}}^{(k)}}{2\sigma^2} \right) p^{-\omega_k \sum_{j \in [p]} \mathbb{1}\{m_j = k\}} \right\}.$$

A.1 Preliminary for Proof of Posterior Consistency

In this section we prove lemmas that will be needed in the posterior consistency proof later. Recall that the superscript (k) is dropped for ease of notation. For $\mathbf{r}, \mathbf{s} \in \{0, 1\}^p$, we use $\mathbf{r} \setminus \mathbf{s}$ to denote the set (or the corresponding indicator vector) such that $j \in \mathbf{r} \setminus \mathbf{s}$ if and only if $r_j = 1$ and $s_j = 0$.

Lemma 1. *Under Conditions (2a) and (2b), for any $\mathbf{r}, \mathbf{s} \in \{0, 1\}^p$ the following hold.*

1. *If $S_{\mathbf{r}} \subset S_{\mathbf{s}}$, we have*

$$\frac{D_{\mathbf{r}}}{D_{\mathbf{s}}} \leq (1 + n\tilde{\sigma}_0^2)^{|\mathbf{s} \setminus \mathbf{r}|/2}.$$

2. *If $S_{\mathbf{s}} \subset S_{\mathbf{r}}$, we have*

$$\frac{D_{\mathbf{r}}}{D_{\mathbf{s}}} \leq 1.$$

Proof. For the first case, we have

$$\begin{aligned} \frac{D_{\mathbf{r}}^2}{D_{\mathbf{s}}^2} &= \left| (\mathbf{I} + \tilde{\sigma}_0^2 \mathbf{X}_{\mathbf{r}} \mathbf{X}_{\mathbf{r}}^T)^{-1} \left(\mathbf{I} + \tilde{\sigma}_0^2 \mathbf{X}_{\mathbf{r}} \mathbf{X}_{\mathbf{r}}^T + \tilde{\sigma}_0^2 \mathbf{X}_{\mathbf{s} \setminus \mathbf{r}} \mathbf{X}_{\mathbf{s} \setminus \mathbf{r}}^T \right) \right| \\ &= \left| \mathbf{I} + (\mathbf{I} + \tilde{\sigma}_0^2 \mathbf{X}_{\mathbf{r}} \mathbf{X}_{\mathbf{r}}^T)^{-1} \left(\tilde{\sigma}_0^2 \mathbf{X}_{\mathbf{s} \setminus \mathbf{r}} \mathbf{X}_{\mathbf{s} \setminus \mathbf{r}}^T \right) \right| \\ &= \left| \mathbf{I} + \tilde{\sigma}_0^2 \mathbf{X}_{\mathbf{s} \setminus \mathbf{r}}^T (\mathbf{I} + \tilde{\sigma}_0^2 \mathbf{X}_{\mathbf{r}} \mathbf{X}_{\mathbf{r}}^T)^{-1} \mathbf{X}_{\mathbf{s} \setminus \mathbf{r}} \right| \\ &\leq \left| \mathbf{I} + \tilde{\sigma}_0^2 \mathbf{X}_{\mathbf{s} \setminus \mathbf{r}}^T \mathbf{X}_{\mathbf{s} \setminus \mathbf{r}} \right|, \end{aligned}$$

where the third equation follows from Sylvester's determinant theorem and the last inequality follows from the fact that if $\mathbf{A}, \mathbf{B}, \mathbf{A} - \mathbf{B}$ are all positive definite, then $|\mathbf{A}| > |\mathbf{B}|$. Letting $\lambda_i(\mathbf{A})$ denote the i -th eigenvalue of the matrix \mathbf{A} . Recall that

$$|\mathbf{I} + \tilde{\sigma}_0^2 \mathbf{X}_{\mathbf{s} \setminus \mathbf{r}}^T \mathbf{X}_{\mathbf{s} \setminus \mathbf{r}}| = \prod_{i=1}^{|\mathbf{s} \setminus \mathbf{r}|} \lambda_i(\mathbf{I} + \tilde{\sigma}_0^2 \mathbf{X}_{\mathbf{s} \setminus \mathbf{r}}^T \mathbf{X}_{\mathbf{s} \setminus \mathbf{r}}). \quad (23)$$

By Condition (2a),

$$\sum_{i=1}^{|\mathbf{s} \setminus \mathbf{r}|} \lambda_i(\mathbf{I} + \tilde{\sigma}_0^2 \mathbf{X}_{\mathbf{s} \setminus \mathbf{r}}^T \mathbf{X}_{\mathbf{s} \setminus \mathbf{r}}) = \text{Trace}(\mathbf{I} + \tilde{\sigma}_0^2 \mathbf{X}_{\mathbf{s} \setminus \mathbf{r}}^T \mathbf{X}_{\mathbf{s} \setminus \mathbf{r}}) = |\mathbf{s} \setminus \mathbf{r}|(1 + n\tilde{\sigma}_0^2).$$

By the inequality of geometric and arithmetic means, this shows that (23) is bounded from above by $(1 + n\tilde{\sigma}_0^2)^{|\mathbf{s} \setminus \mathbf{r}|}$. This yields the first bound given in the lemma.

For the second case, we have

$$\begin{aligned} \frac{D_{\mathbf{r}}^2}{D_{\mathbf{s}}^2} &= \left| (\mathbf{I} + \tilde{\sigma}_0^2 \mathbf{X}_{\mathbf{r}} \mathbf{X}_{\mathbf{r}}^T)^{-1} \left(\mathbf{I} + \tilde{\sigma}_0^2 \mathbf{X}_{\mathbf{r}} \mathbf{X}_{\mathbf{r}}^T - \tilde{\sigma}_0^2 \mathbf{X}_{\mathbf{r} \setminus \mathbf{s}} \mathbf{X}_{\mathbf{r} \setminus \mathbf{s}}^T \right) \right| \\ &= \left| \mathbf{I} - (\mathbf{I} + \tilde{\sigma}_0^2 \mathbf{X}_{\mathbf{r}} \mathbf{X}_{\mathbf{r}}^T)^{-1} \left(\tilde{\sigma}_0^2 \mathbf{X}_{\mathbf{r} \setminus \mathbf{s}} \mathbf{X}_{\mathbf{r} \setminus \mathbf{s}}^T \right) \right| \\ &\leq 1. \end{aligned}$$

The proof is complete. □

The next lemma bounds the difference between $R_{\mathbf{r}}$ and $R_{\mathbf{r}}^*$.

Lemma 2. *Under Conditions (1a), (2a) and (4), we have*

1. $\mathbb{P}[\frac{1}{2}n\sigma^2 \leq \|\mathbf{e}\|_2^2 \leq \frac{3}{2}n\sigma^2] \geq 1 - 2p^{-1}$.
2. $\mathbb{P}[\|\mathbf{y}\|_2^2 \leq 3n\sigma^2 B_1 \log p] \geq 1 - 2p^{-1}$.
3. $\mathbb{P}[R_{\mathbf{r}} - R_{\mathbf{r}}^* \leq 3B_1\sigma^2 \log p / (\nu\tilde{\sigma}_0^2)] \geq 1 - 2p^{-1}$ for any index r .

Remark. Since we assume K is fixed, by a union bound, it follows that with probability at least $1 - 2Kp^{-1} = 1 - O(p^{-1})$, $\frac{1}{2}n\sigma^2 \leq \|\mathbf{e}^{(k)}\|_2^2 \leq \frac{3}{2}n\sigma^2$ for all $k = 1, \dots, K$. The other two statements can be extended to all K data sets analogously.

Proof. For part 1, we know that $\|\mathbf{e}\|_2^2/\sigma^2 \sim \chi_n^2$. By the concentration of the chi-square distribution and Condition (4), we have

$$\mathbb{P}\left[\left|\frac{\|\mathbf{e}\|_2^2}{n\sigma^2} - 1\right| \geq \frac{1}{2}\right] \leq 2e^{-n/25} \leq 2p^{-1},$$

which implies

$$\mathbb{P}\left[\frac{1}{2}n\sigma^2 \leq \|\mathbf{e}\|_2^2 \leq \frac{3}{2}n\sigma^2\right] \geq 1 - 2p^{-1}.$$

For part 2, by the Cauchy-Schwartz inequality,

$$\|\mathbf{y}\|_2^2 = \|\mathbf{X}\boldsymbol{\beta}^* + \mathbf{e}\|_2^2 \leq 2\|\mathbf{X}\boldsymbol{\beta}^*\|_2^2 + 2\|\mathbf{e}\|_2^2.$$

Using part 1, we obtain that

$$\mathbb{P}[\|\mathbf{y}\|_2^2 \geq 2\|\mathbf{X}\boldsymbol{\beta}^*\|_2^2 + 3n\sigma^2] \leq 2p^{-1}.$$

The bound then can be proved by invoking Condition (1a).

For part 3, by the Sherman-Morrison-Woodbury identity, we have

$$\begin{aligned} 0 \leq R_{\mathbf{r}} - R_{\mathbf{r}}^* &= \mathbf{y}^T \mathbf{X}_{\mathbf{r}} ((\mathbf{X}_{\mathbf{r}}^T \mathbf{X}_{\mathbf{r}})^{-1} - (\mathbf{X}_{\mathbf{r}}^T \mathbf{X}_{\mathbf{r}} + \tilde{\sigma}_0^2 \mathbf{I})^{-1}) \mathbf{X}_{\mathbf{r}}^T \mathbf{y}^T \\ &= \mathbf{y}^T \mathbf{X}_{\mathbf{r}} (\mathbf{X}_{\mathbf{r}}^T \mathbf{X}_{\mathbf{r}})^{-1} (\tilde{\sigma}_0^2 \mathbf{I} + (\mathbf{X}_{\mathbf{r}}^T \mathbf{X}_{\mathbf{r}})^{-1})^{-1} (\mathbf{X}_{\mathbf{r}}^T \mathbf{X}_{\mathbf{r}})^{-1} \mathbf{X}_{\mathbf{r}}^T \mathbf{y} \\ &\leq (n\tilde{\sigma}_0^2)^{-1} n \mathbf{y}^T \mathbf{X}_{\mathbf{r}} (\mathbf{X}_{\mathbf{r}}^T \mathbf{X}_{\mathbf{r}})^{-2} \mathbf{X}_{\mathbf{r}}^T \mathbf{y}. \end{aligned}$$

The last inequality is due to the fact that $\tilde{\sigma}_0^2 \mathbf{I} \preceq \tilde{\sigma}_0^2 \mathbf{I} + (\mathbf{X}_{\mathbf{r}}^T \mathbf{X}_{\mathbf{r}})^{-1}$. Let $\mathbf{M} = n \mathbf{X}_{\mathbf{r}} (\mathbf{X}_{\mathbf{r}}^T \mathbf{X}_{\mathbf{r}})^{-2} \mathbf{X}_{\mathbf{r}}^T$, where the notation $\mathbf{A} \preceq \mathbf{B}$ means $\mathbf{B} - \mathbf{A}$ is positive semidefinite. By Condition (2b),

$$\lambda_{\max}(\mathbf{M}) = \lambda_{\max}(n(\mathbf{X}_{\mathbf{r}}^T \mathbf{X}_{\mathbf{r}})^{-1}) \leq \frac{1}{\nu}.$$

That is, \mathbf{M} has bounded eigenvalues. Thus, by part 2,

$$\begin{aligned} \mathbb{P}\left[R_{\mathbf{r}} - R_{\mathbf{r}}^* \geq \frac{3B_1\sigma^2 \log p}{\tilde{\sigma}_0^2 \nu}\right] &\leq \mathbb{P}\left[\mathbf{y}^T \mathbf{M} \mathbf{y} \geq \frac{3nB_1\sigma^2 \log p}{\nu}\right] \\ &\leq \mathbb{P}[\|\mathbf{y}\|_2^2 \geq 3B_1n\sigma^2 \log p] \leq 2p^{-1}, \end{aligned}$$

which completes the proof. \square

The third lemma is to bound the quadratic forms of residuals.

Lemma 3. *Under Conditions (2a) and (2c), the following hold.*

1. *For any distinct pair $(\mathbf{r}_1, \mathbf{r}_2)$ satisfying $\mathbf{r}_1 \subset \mathbf{r}_2$ and $|\mathbf{r}_2| \leq L$, we have*

$$\lambda_{\min} \left(\mathbf{X}_{\mathbf{r}_2 \setminus \mathbf{r}_1}^T (\mathbf{I}_n - \Psi_{\mathbf{r}_1}) \mathbf{X}_{\mathbf{r}_2 \setminus \mathbf{r}_1} \right) \geq n\nu.$$

2. *For any distinct pair $(\mathbf{r}_1, \mathbf{r}_2)$ satisfying $\mathbf{r}_1 \subset \mathbf{r}_2$ and $|\mathbf{r}_2| \leq L$, we have*

$$\mathbb{P} \left[\max_{\mathbf{r}_1 \subset \mathbf{r}_2} \frac{\mathbf{e}^T (\Psi_{\mathbf{r}_2} - \Psi_{\mathbf{r}_1}) \mathbf{e}}{|\mathbf{r}_2| - |\mathbf{r}_1|} \leq B_3 \sigma^2 \log p \right] \geq 1 - p^{-1}.$$

Proof. For part 1, if we write $\mathbf{X}_{\mathbf{r}_2} = [\mathbf{X}_{\mathbf{r}_1}, \mathbf{X}_{\mathbf{r}_2 \setminus \mathbf{r}_1}]$, by the inverse of the block matrix, the lower right component of $(n^{-1} \mathbf{X}_{\mathbf{r}_2}^T \mathbf{X}_{\mathbf{r}_2}^{-1})^{-1}$ is $(n^{-1} \mathbf{X}_{\mathbf{r}_2 \setminus \mathbf{r}_1}^T (\mathbf{I}_n - \Psi_{\mathbf{r}_1}) \mathbf{X}_{\mathbf{r}_2 \setminus \mathbf{r}_1})^{-1}$, which implies the bound.

For part 2, by the block matrix inversion formula, we have

$$\Psi_{\mathbf{r} \cup \{k\}} - \Psi_{\mathbf{r}} = \frac{(\mathbf{I} - \Psi_{\mathbf{r}}) \mathbf{X}_k \mathbf{X}_k^T (\mathbf{I} - \Psi_{\mathbf{r}})}{\mathbf{X}_k^T (\mathbf{I} - \Psi_{\mathbf{r}}) \mathbf{X}_k}.$$

Hence,

$$\mathbf{e}^T (\Psi_{\mathbf{r} \cup \{k\}} - \Psi_{\mathbf{r}}) \mathbf{e} = \frac{(\mathbf{e}^T (\mathbf{I} - \Psi_{\mathbf{r}}) \mathbf{X}_k)^2 / n}{\mathbf{X}_k^T (\mathbf{I} - \Psi_{\mathbf{r}}) \mathbf{X}_k / n}.$$

Due to part 1, the denominator $\mathbf{X}_k^T (\mathbf{I} - \Psi_{\mathbf{r}}) \mathbf{X}_k / n \geq \nu$. For the numerator, define the random variable

$$V(Z) := \max_{|\mathbf{r}| \leq L, k \notin \mathbf{r}} \frac{1}{\sqrt{n}} |Z^T (\mathbf{I} - \Psi_{\mathbf{r}}) \mathbf{X}_k|,$$

where $Z \sim \mathcal{N}(0, \mathbf{I}_n)$. For any two vectors $Z, Z' \in \mathbb{R}^n$, by Condition (2a),

$$\begin{aligned} |V(Z) - V(Z')| &\leq \max_{|\mathbf{r}| \leq L, k \notin \mathbf{r}} \frac{1}{\sqrt{n}} |(Z - Z')^T (\mathbf{I} - \Psi_{\mathbf{r}}) \mathbf{X}_k| \\ &\leq \frac{1}{\sqrt{n}} \|(\mathbf{I} - \Psi_{\mathbf{r}}) \mathbf{X}_k\|_2 \|Z - Z'\|_2 \leq \|Z - Z'\|_2. \end{aligned}$$

Thus, by the concentration of measures for Lipschitz functions of Gaussian random variables, we have

$$\mathbb{P}[V(Z) \geq \mathbb{E}[V(Z)] + t] \leq \exp(-t^2/2).$$

Due to Condition (2c),

$$\mathbb{E}[V(Z)] \leq \frac{1}{2} \sqrt{B_3 \nu \log p}.$$

Thus,

$$\mathbb{P} \left[V(Z) \geq \frac{1}{2} \sqrt{B_3 \nu \log p} + \frac{1}{2} \sqrt{B_3 \nu \log p} \right] \leq \exp \left(-\frac{1}{8} B_3 \nu \log p \right) \leq p^{-1}.$$

Hence,

$$\mathbb{P} \left[\max_{|\mathbf{r}| \leq L, k \notin \mathbf{r}} \mathbf{e}^T (\Psi_{\mathbf{r} \cup \{k\}} - \Psi_{\mathbf{r}}) \mathbf{e} \geq B_3 \sigma^2 \log p \right] \leq p^{-1},$$

which implies part 2. □

A.2 Proof of Posterior Consistency

We prove the posterior consistency in this section. For simplicity, all universal constants other than c_1 , c_2 and c_3 are denoted by C or C' .

Proof. We divide the proof into two parts depending on whether the model being considered is overfitted or underfitted. First, consider the overfitted case. Let

$$\mathbb{M}_{1r} = \{\mathbf{r} \in \{0, 1\}^{Kp} : \mathbf{r} \in \mathbb{M}_r, \quad \mathbf{r}^* \subset \mathbf{r}\}$$

denote the collection of all models other than the true model \mathbf{r}^* that include all influential covariates. Hence, for any $\mathbf{r} \in \mathbb{M}_{1r}$, $l = |\mathbf{r} \setminus \mathbf{r}^*| \geq 1$. Recalling that $\mathcal{M}_j = \{k \in [K] : r_j^{(k)} = 1\}$ and $m_j = |\mathcal{M}_j|$, denote

$$l_k = \sum_{j \in [p]} \mathbb{1}\{m_j = k\} \quad (24)$$

and similarly define $l_k^* = \sum_{j \in [p]} \mathbb{1}\{m_j^* = k\}$. It follows that

$$\sum_{k=1}^K |\mathbf{r}^{(k)}| = \sum_{k=1}^K k l_k,$$

which implies that

$$\sum_{k=1}^K |\mathbf{r}^{(k)} \setminus \mathbf{r}^{(k)*}| = \sum_{k=1}^K k(l_k - l_k^*). \quad (25)$$

Given indicator vector \mathbf{r} , we have $\gamma(\mathbf{r})$ defined in (4). In the overfitted case, we have

$$|\gamma| - |\gamma^*| = \sum_{k=1}^K (l_k - l_k^*) \leq \sum_{k=1}^K |\mathbf{r}^{(k)} \setminus \mathbf{r}^{(k)*}| =: l. \quad (26)$$

By (26), Lemma 1, and Conditions (3a), (3b) and (3d), we have

$$\begin{aligned} \frac{\Pi(\mathbf{r} | (\mathbf{y}^{(k)})_{k \in [K]})}{\Pi(\mathbf{r}^* | (\mathbf{y}^{(k)})_{k \in [K]})} &= \frac{f(|\gamma|, L)}{f(|\gamma^*|, L)} \prod_{k=1}^K \left(p^{-(l_k - l_k^*)\omega_k} \right) \prod_{k=1}^K \left(\frac{D_{\mathbf{r}^{(k)}} \exp\left(-\frac{1}{2\sigma^2} R_{\mathbf{r}^{(k)}}^{(k)}\right)}{D_{\mathbf{r}^{(k)*}} \exp\left(-\frac{1}{2\sigma^2} R_{\mathbf{r}^{(k)*}}^{(k)}\right)} \right) \\ &\leq C p^{l\beta} p^{-\sum_{k=1}^K (l_k - l_k^*)\omega_k} \prod_{k=1}^K \exp\left(-\frac{1}{2\sigma^2} \left(R_{\mathbf{r}^{(k)}}^{(k)} - R_{\mathbf{r}^{(k)*}}^{(k)}\right)\right). \end{aligned}$$

By Condition (1b) and Lemma 3, if $|\mathbf{r} \setminus \mathbf{r}^*| \geq 1$, we have

$$\begin{aligned} R_{\mathbf{r}^*}^* - R_{\mathbf{r}}^* &= \|(\Psi_{\mathbf{r}} - \Psi_{\mathbf{r}^*})\mathbf{y}\|_2^2 = \|(\Psi_{\mathbf{r}} - \Psi_{\mathbf{r}^*})\mathbf{X}_{-\mathbf{r}^*}\beta_{-\mathbf{r}^*}^* + (\Psi_{\mathbf{r}} - \Psi_{\mathbf{r}^*})\mathbf{e}\|_2^2 \\ &\leq 2\|(\Psi_{\mathbf{r}} - \Psi_{\mathbf{r}^*})\mathbf{X}_{-\mathbf{r}^*}\beta_{-\mathbf{r}^*}^*\|_2^2 + 2\|(\Psi_{\mathbf{r}} - \Psi_{\mathbf{r}^*})\mathbf{e}\|_2^2 \\ &\leq 2B_2\sigma^2 \log p + 2|\mathbf{r} \setminus \mathbf{r}^*|B_3\sigma^2 \log p, \end{aligned}$$

with probability at least $1 - c_2 p^{-c_3}$ or some universal constants $c_2, c_3 > 0$. Combining with Lemma 2, we have

$$\begin{aligned} R_{\mathbf{r}^*} - R_{\mathbf{r}} &\leq R_{\mathbf{r}^*} - R_{\mathbf{r}}^* = R_{\mathbf{r}^*} - R_{\mathbf{r}^*}^* + R_{\mathbf{r}^*}^* - R_{\mathbf{r}}^* \\ &\leq 3B_1 \log p \sigma^2 / (\nu \tilde{\sigma}_0^2) + 2B_2 \sigma^2 \log p + 2|\mathbf{r} \setminus \mathbf{r}^*|B_3 \sigma^2 \log p \\ &\leq 3|\mathbf{r} \setminus \mathbf{r}^*| (B_1 / (\nu \tilde{\sigma}_0^2) + B_2 + B_3) \sigma^2 \log p, \end{aligned}$$

for all K data sets with probability at least $1 - c_2 p^{-c_3}$.

By Equation (8) and Condition (3c), the posterior ratio becomes

$$\begin{aligned} \frac{\Pi(\mathbf{r} | (\mathbf{y}^{(k)})_{k \in [K]})}{\Pi(\mathbf{r}^* | (\mathbf{y}^{(k)})_{k \in [K]})} &\leq C p^{l\beta} p^{-\sum_{k=1}^K (l_k - l_k^*) \omega_k} p^{\sum_{k=1}^K 3|\mathbf{r}^{(k)} \setminus \mathbf{r}^{(k)*}| (B_1/(\nu \tilde{\sigma}_0^2) + B_2 + B_3)/2} \\ &= C p^{\beta \sum_{k=1}^K k(l_k - l_k^*)} p^{-\sum_{k=1}^K k(l_k - l_k^*) (\omega_k/k)} p^{(3(B_1/(\nu \tilde{\sigma}_0^2) + B_2 + B_3)/2) \sum_{k=1}^K k(l_k - l_k^*)} \\ &\leq C p^{-2 \sum_{k=1}^K |\mathbf{r}^{(k)} \setminus \mathbf{r}^{(k)*}|} = C p^{-2|\mathbf{r} \setminus \mathbf{r}^*|}, \end{aligned}$$

with probability at least $1 - c_2 p^{-c_3}$, where we have used (25) in the second equality and the third inequality. Hence,

$$\begin{aligned} \frac{\Pi(\mathbb{M}_1 | (\mathbf{y}^{(k)})_{k \in [K]})}{\Pi(\mathbf{r}^* | (\mathbf{y}^{(k)})_{k \in [K]})} &= \sum_{\mathbf{r} \in \mathbb{M}_{1r}} \frac{\Pi(\mathbf{r} | (\mathbf{y}^{(k)})_{k \in [K]})}{\Pi(\mathbf{r}^* | (\mathbf{y}^{(k)})_{k \in [K]})} \\ &\leq \sum_{l=1}^{\infty} C(Kp)^l p^{-2l} \leq C' p^{-1}, \end{aligned} \tag{27}$$

with probability at least $1 - c_2 p^{-c_3}$, where the first inequality in (27) follows from the fact that there are at most $(Kp)^l$ models that satisfy $\sum_{k=1}^K |\mathbf{r}^{(k)} \setminus \mathbf{r}^{(k)*}| = l$.

Second, consider the underfitted case. Let

$$\mathbb{M}_{2r} = \{\mathbf{r} \in \{0, 1\}^{Kp} : \mathbf{r} \in \mathbb{M}_r, \quad |\mathbf{r}^* \setminus \mathbf{r}| \geq 1\},$$

be the collection of models which do not include at least one influential covariate. Fix an arbitrary $\mathbf{r} \in \mathbb{M}_{2r}$, and let $l = |\mathbf{r}^* \setminus \mathbf{r}|$, $\tilde{\mathbf{r}} = \mathbf{r} \cup \mathbf{r}^*$ and $l_0 = |\mathbf{r}|$. Then, $|\tilde{\mathbf{r}} \setminus \mathbf{r}| = l$ and $|\tilde{\mathbf{r}} \setminus \mathbf{r}^*| = l + l_0 - |\mathbf{r}^*|$. Let $\tilde{\mathbf{r}}^{(k)}$ be defined analogously for each $k \in [K]$, and let $\tilde{\gamma} = \gamma(\tilde{\mathbf{r}})$. Let $\tilde{\mathcal{M}}_j$, \tilde{m}_j and \tilde{l}_k be defined in the same manner as (24). Then, $|\gamma| \leq |\tilde{\gamma}|$ and

$$\sum_{k=1}^K |\tilde{\mathbf{r}}^{(k)} \setminus \mathbf{r}^{(k)}| = \sum_{k=1}^K k(\tilde{l}_k - l_k).$$

By Lemma 1, Conditions (3a), (3b) and (3d),

$$\begin{aligned} \frac{\Pi(\mathbf{r} | (\mathbf{y}^{(k)})_{k \in [K]})}{\Pi(\tilde{\mathbf{r}} | (\mathbf{y}^{(k)})_{k \in [K]})} &= \frac{f(|\gamma|, L)}{f(|\tilde{\gamma}|, L)} \prod_{k=1}^K \left(p^{(\tilde{l}_k - l_k) \omega_k} \frac{D_{\mathbf{r}^{(k)}} \exp\left(-\frac{1}{2\sigma^2} R_{\mathbf{r}^{(k)}}^{(k)}\right)}{D_{\tilde{\mathbf{r}}^{(k)}} \exp\left(-\frac{1}{2\sigma^2} R_{\tilde{\mathbf{r}}^{(k)}}^{(k)}\right)} \right) \\ &\leq C p^{\sum_{k=1}^K |\tilde{\mathbf{r}}^{(k)} \setminus \mathbf{r}^{(k)}| \alpha} p^{\sum_{k=1}^K (\tilde{l}_k - l_k) \omega_k} \prod_{k=1}^K \exp\left(-\frac{1}{2\sigma^2} (R_{\mathbf{r}^{(k)}}^{(k)} - R_{\tilde{\mathbf{r}}^{(k)}}^{(k)})\right). \end{aligned}$$

By Condition (1b) and Lemma 3, if $|\tilde{\mathbf{r}}^{(k)} \setminus \mathbf{r}^{(k)}| \geq 1$, we have, with probability at least $1 - c_2 p^{-c_3}$

$$\begin{aligned} R_{\mathbf{r}}^* - R_{\tilde{\mathbf{r}}}^* &= \mathbf{y}^T (\Psi_{\tilde{\mathbf{r}}} - \Psi_{\mathbf{r}}) \mathbf{y} = \|(\Psi_{\tilde{\mathbf{r}}} - \Psi_{\mathbf{r}}) (\mathbf{X}_{\mathbf{r}^*} \beta_{\mathbf{r}^*}^* + \mathbf{X}_{-\mathbf{r}^*} \beta_{-\mathbf{r}^*}^* + \mathbf{e})\|_2^2 \\ &\geq (\|(\Psi_{\tilde{\mathbf{r}}} - \Psi_{\mathbf{r}}) \mathbf{X}_{\mathbf{r}^*} \beta_{\mathbf{r}^*}^*\|_2 - \|(\Psi_{\tilde{\mathbf{r}}} - \Psi_{\mathbf{r}}) \mathbf{X}_{-\mathbf{r}^*} \beta_{-\mathbf{r}^*}^*\|_2 + \|(\Psi_{\tilde{\mathbf{r}}} - \Psi_{\mathbf{r}}) \mathbf{e}\|_2)^2 \\ &\geq \left(\|(\Psi_{\tilde{\mathbf{r}}} - \Psi_{\mathbf{r}}) \mathbf{X}_{\mathbf{r}^*} \beta_{\mathbf{r}^*}^*\|_2 - \sqrt{B_2 \sigma^2 \log p} - \sqrt{|\tilde{\mathbf{r}} \setminus \mathbf{r}| B_3 \sigma^2 \log p} \right)^2, \end{aligned}$$

where the superscript (k) has been dropped. Due to Condition (5) and Lemma 3, we have

$$\begin{aligned}
\|(\Psi_{\tilde{\mathbf{r}}} - \Psi_{\mathbf{r}}) \mathbf{X}_{\mathbf{r}^*} \beta_{\mathbf{r}^*}^*\|_2^2 &= \|(\mathbf{I} - \Psi_{\mathbf{r}}) \mathbf{X}_{\mathbf{r}^*} \beta_{\mathbf{r}^*}^*\|_2^2 \\
&= \|(\mathbf{I} - \Psi_{\mathbf{r}}) \mathbf{X}_{\mathbf{r}^* \setminus \mathbf{r}} \beta_{\mathbf{r}^* \setminus \mathbf{r}}^*\|_2^2 \\
&\geq n\nu \|\beta_{\mathbf{r}^* \setminus \mathbf{r}}^*\|_2^2 \\
&\geq 8 \left| \mathbf{r}^{(k)*} \setminus \mathbf{r}^{(k)} \right| (B_2 + B_3) \sigma^2 \log p.
\end{aligned}$$

Thus,

$$R_{\mathbf{r}}^* - R_{\tilde{\mathbf{r}}}^* \geq \frac{1}{4} \|(\Psi_{\tilde{\mathbf{r}}} - \Psi_{\mathbf{r}}) \mathbf{X}_{\mathbf{r}^*} \beta_{\mathbf{r}^*}^*\|_2^2,$$

with probability at least $1 - c_2 p^{-c_3}$. Combining with Lemma 2, we have

$$R_{\mathbf{r}} - R_{\tilde{\mathbf{r}}} \geq R_{\mathbf{r}}^* - R_{\tilde{\mathbf{r}}}^* + R_{\tilde{\mathbf{r}}}^* - R_{\tilde{\mathbf{r}}} \geq \frac{n\nu \|\beta_{\mathbf{r}^* \setminus \mathbf{r}}^*\|_2^2}{4} - \frac{3B_1 \sigma^2 \log p}{\nu \tilde{\sigma}_0^2},$$

with probability at least $1 - c_2 p^{-c_3}$. Observe that

$$\sum_{k=1}^K \|\beta_{\mathbf{r}^{(k)*} \setminus \mathbf{r}^{(k)}}^*\|_2^2 \geq \sum_{j \in [p]} |\mathcal{M}_j^* \setminus \mathcal{M}_j| C_{\beta, m_j^*}.$$

Due to Condition (5) and Equation (8), the posterior ratio becomes

$$\begin{aligned}
\frac{\Pi(\mathbf{r} | (\mathbf{y}^{(k)})_{k \in [K]})}{\Pi(\tilde{\mathbf{r}} | (\mathbf{y}^{(k)})_{k \in [K]})} &\leq p^{\sum_{k=1}^K |\tilde{\mathbf{r}}^{(k)} \setminus \mathbf{r}^{(k)}| \alpha} p^{\sum_{k=1}^K \omega_k (\tilde{l}_k - l_k)} p^{-\sum_{k=1}^K |\mathbf{r}^{(k)*} \setminus \mathbf{r}^{(k)}| (\alpha+2)} p^{-\sum_{j \in [p]} |\mathcal{M}_j^* \setminus \mathcal{M}_j| (\omega_{m_j^*} / m_j^*)} \\
&\leq C p^{-2 \sum_{k=1}^K |\tilde{\mathbf{r}}^{(k)} \setminus \mathbf{r}^{(k)}|},
\end{aligned}$$

where in the last inequality we have used

$$\sum_{k=1}^K \omega_k (\tilde{l}_k - l_k) - \sum_{j \in [p]} |\mathcal{M}_j^* \setminus \mathcal{M}_j| (\omega_{m_j^*} / m_j^*) \leq 0, \quad (28)$$

for which we will give a proof at the end. By the result for the overfitted case, the posterior ratio becomes

$$\begin{aligned}
\frac{\Pi(\mathbf{r} | (\mathbf{y}^{(k)})_{k \in [K]})}{\Pi(\mathbf{r}^* | (\mathbf{y}^{(k)})_{k \in [K]})} &= \frac{\Pi(\mathbf{r} | (\mathbf{y}^{(k)})_{k \in [K]})}{\Pi(\tilde{\mathbf{r}} | (\mathbf{y}^{(k)})_{k \in [K]})} \frac{\Pi(\tilde{\mathbf{r}} | (\mathbf{y}^{(k)})_{k \in [K]})}{\Pi(\mathbf{r}^* | (\mathbf{y}^{(k)})_{k \in [K]})} \\
&\leq C p^{-2(\sum_{k=1}^K |\mathbf{r}^{(k)} \setminus \mathbf{r}^{(k)*}| + \sum_{k=1}^K |\mathbf{r}^{(k)*} \setminus \mathbf{r}^{(k)}|)},
\end{aligned}$$

with probability at least $1 - c_2 p^{-c_3}$. It follows that

$$\begin{aligned}
\frac{\Pi(\mathbb{M}_2 | (\mathbf{y}^{(k)})_{k \in [K]})}{\Pi(\mathbf{r}^* | (\mathbf{y}^{(k)})_{k \in [K]})} &= \sum_{\mathbf{r} \in \mathbb{M}_{2r}} \frac{\Pi(\mathbf{r} | (\mathbf{y}^{(k)})_{k \in [K]})}{\Pi(\mathbf{r}^* | (\mathbf{y}^{(k)})_{k \in [K]})} \\
&\leq \sum_{l_1=0}^{\infty} \sum_{l_2=1}^{\infty} C(Kp)^{l_1+l_2} p^{-2l_1-2l_2} \leq C' p^{-1}.
\end{aligned} \quad (29)$$

with probability at least $1 - c_2 p^{-c_3}$, where the first inequality is due to that there are at most $(Kp)^{l_1+l_2}$ models such that $|\mathbf{r} \setminus \mathbf{r}^*| = l_1$ and $|\mathbf{r}^* \setminus \mathbf{r}| = l_2$.

Combining (27) and (29), we have

$$\Pi(\mathbf{r}^* | (\mathbf{y}^{(k)})_{k \in [K]}) \geq 1 - c_1 p^{-1},$$

with probability at least $1 - c_2 p^{-c_3}$, where $c_1 > 0$ is some universal constant.

Finally, we prove (28) via induction. When $|\mathbf{r}^* \setminus \mathbf{r}| = l = 1$, \mathbf{r} misses one influential covariate. Let's assume that \mathbf{r} misses one covariate i (in one data set) and $\tilde{m}_i = k_0 \geq m_i^* \geq 1$. Then,

$$\sum_{k=1}^K \omega_k (\tilde{l}_k - l_k) = \omega_{k_0} - \omega_{k_0-1},$$

where we define $\omega_0 = 0$. Besides, notice that

$$\sum_{j \in [p]} |\mathcal{M}_j^* \setminus \mathcal{M}_j| (\omega_{m_j^*} / m_j^*) = \omega_{m_i^*} / m_i^*.$$

It follows from (8) that

$$\omega_{k_0} - \omega_{k_0-1} - \omega_{m_i^*} / m_i^* \begin{cases} = 0, & \text{if } k_0 = 1, \\ < \frac{k_0 \omega_{k_0-1}}{k_0-1} - \omega_{k_0-1} - \frac{\omega_{k_0-1}}{k_0-1} = 0, & \text{if } k_0 > 1, \end{cases}$$

which completes the proof for $l = 1$.

Assume that the claim holds for $l = l_0$ and now we prove it also holds for $l = l_0 + 1$. Without loss of generality, assume that $\gamma_i^{(j)*} = 1$ for some $j \in [K]$. Let $\tilde{\mathbf{r}}$ be such that the only difference between $\tilde{\mathbf{r}}$ and $\tilde{\mathbf{r}} = \mathbf{r} \cup \mathbf{r}^*$ is that $\tilde{\mathbf{r}}_i^{(j)} = 0$ but $\tilde{\mathbf{r}}_i^{(j)} \neq 0$. Define $\check{\mathcal{M}}_j$ and \check{m}_j similarly to \mathcal{M}_j and m_j . Observe that for any $j \in [p]$, $\mathcal{M}_j^* \setminus \mathcal{M}_j$ is the disjoint union of $\mathcal{M}_j^* \setminus \check{\mathcal{M}}_j$ and $\check{\mathcal{M}}_j \setminus \mathcal{M}_j$. Hence,

$$\begin{aligned} & \sum_{k=1}^K \omega_k (\tilde{l}_k - l_k) - \sum_{j \in [p]} |\mathcal{M}_j^* \setminus \mathcal{M}_j| (\omega_{m_j^*} / m_j^*) \\ &= \left(\sum_{k=1}^K \omega_k (\tilde{l}_k - \check{l}_k) - \sum_{j \in [p]} |\mathcal{M}_j^* \setminus \check{\mathcal{M}}_j| (\omega_{m_j^*} / m_j^*) \right) + \left(\sum_{k=1}^K \omega_k (\check{l}_k - l_k) - \sum_{j \in [p]} |\check{\mathcal{M}}_j \setminus \mathcal{M}_j| (\omega_{m_j^*} / m_j^*) \right) \end{aligned}$$

where the first term is non-positive since it corresponds to the case $l = 1$, and the second term is non-positive due to the induction assumption. This proves (28). \square

B Fitting muSuSiE

B.1 Iterative Bayesian Stepwise Selection Algorithm

Consider the muSER model defined in (12). To find its posterior distribution, denote the j -th column of $\mathbf{X}^{(k)}$ by $\mathbf{x}_j^{(k)}$ and define

$$\hat{\beta}_j^{(k)} = \left(\left(\mathbf{x}_j^{(k)} \right)^T \mathbf{x}_j^{(k)} \right)^{-1} \left(\mathbf{x}_j^{(k)} \right)^T \mathbf{y}^{(k)}, \quad s_{j(k)}^2 = \frac{\sigma^2}{(\mathbf{x}_j^{(k)})^T \mathbf{x}_j^{(k)}}, \quad z_{j(k)} = \frac{\hat{\beta}_j^{(k)}}{s_{j(k)}}.$$

Let the Bayes Factor (BF) for activating covariate j in the k -th data set be

$$\text{BF}(j, k) = \frac{P(\mathbf{y}^{(k)} | \mathbf{x}_j^{(k)}, \sigma^2, \sigma_0^2, r_j^{(k)} = 1)}{P(\mathbf{y}^{(k)} | \mathbf{x}_j^{(k)}, \sigma^2, r_j^{(k)} = 0)} = \sqrt{\frac{s_{j(k)}^2}{\sigma_0^2 + s_{j(k)}^2}} \exp\left(\frac{z_{j(k)}^2}{2} \times \frac{\sigma_0^2}{\sigma_0^2 + s_{j(k)}^2}\right).$$

Then, for any $I \in \mathcal{P}_K$, the BF for activating covariate j in all data sets indexed by I is given by

$$\text{BF}(j, I) = \prod_{k \in I} \text{BF}(j, k).$$

It follows that the posterior distribution of $(\gamma, 1 - \phi)$ is

$$(\gamma, 1 - \phi) | (\mathbf{y}^{(k)})_{k \in [K]}, \sigma^2, \sigma_0^2 \sim \text{Multinomial}(1, (\boldsymbol{\alpha}, \alpha_0)),$$

where $\boldsymbol{\alpha} = (\boldsymbol{\alpha}^I)_{I \in \mathcal{P}_K}$ and

$$\begin{aligned} \boldsymbol{\alpha}_j^I &\propto \pi_\phi \pi_{|I|} \text{BF}(j, I) \\ \alpha_0 &\propto 1 - \pi_\phi. \end{aligned}$$

The posterior distribution of $\beta_j^{(k)}$ given $r_j^{(k)} = 1$ and $\phi = 1$ is

$$\beta_j^{(k)} | (\mathbf{y}^{(k)})_{k \in [K]}, \sigma^2, \sigma_0^2 \sim \mathcal{N}(\mu_{1j}^{(k)}, \sigma_{1j(k)}^2),$$

where

$$\sigma_{1j(k)}^2 = \frac{1}{1/s_{j(k)}^2 + 1/\sigma_0^2}, \quad \mu_{1j}^{(k)} = \frac{\sigma_{1j(k)}^2}{s_{j(k)}^2} \times \widehat{\beta}_j^{(k)}.$$

The above calculation shows that to obtain the posterior distribution for the muSER model, we only need to calculate $\text{BF}(j, k)$ for each $j \in [p]$ and $k \in [K]$.

B.1.1 Estimation of σ_{0l}^2

Given σ^2 , we use an empirical bayes approach to estimating the hyperparameters σ_{0l}^2 . Since at most one covariate is activated in (12), in total there are $|\mathcal{P}_K| \times p + 1$ possible models, where 1 indicates the null model. Hence, the likelihood of the variance components σ^2, σ_0^2 under the muSER model is

$$\begin{aligned} \prod_{k=1}^K P(\mathbf{y}^{(k)} | \mathbf{X}^{(k)}, \sigma^2, \sigma_0^2) &= \\ \sum_{I \in \mathcal{P}_K} \sum_{j=1}^p \pi_\phi \pi_{|I|} &\left\{ \prod_{k \in I} P(\mathbf{y}^{(k)} | \mathbf{x}_j^{(k)}, \sigma^2, \sigma_0^2, r_j^{(k)} = 1) \right\} \left\{ \prod_{k \notin I} P(\mathbf{y}^{(k)} | \mathbf{x}_j^{(k)}, \sigma^2, r_j^{(k)} = 0) \right\} \\ &+ (1 - \pi_\phi) \prod_{k=1}^K P(\mathbf{y}^{(k)} | \mathbf{x}_j^{(k)}, \sigma^2, r_j^{(k)} = 0). \end{aligned}$$

We can rewrite the likelihood using the Bayes factors we have defined in the last subsection by

$$\prod_{k=1}^K P(\mathbf{y}^{(k)} | \mathbf{X}^{(k)}, \sigma^2, \sigma_0^2) = \left\{ \prod_{k=1}^K P_0(\mathbf{y}^{(k)} | \sigma^2) \right\} \left\{ \sum_{I \in \mathcal{P}_K} \sum_{j=1}^p \pi_\phi \pi_{|I|} \text{BF}(j, I; \sigma^2, \sigma_0^2) + (1 - \pi_\phi) \right\},$$

where $P_0(\mathbf{y}^{(k)} | \sigma^2) = P(\mathbf{y}^{(k)} | \mathbf{x}_j^{(k)}, \sigma^2, r_j^{(k)} = 0)$ denotes the probability of observing $\mathbf{y}^{(k)}$ under the null model that $\mathbf{r}^{(k)} = 0$, and we write $\text{BF}(j, I; \sigma^2, \sigma_0^2)$ to emphasize that the Bayes factors depend on both σ^2 and σ_0^2 . Thus, by removing the terms that do not involve σ_0^2 , we can define an empirical Bayes estimator of σ_0^2 as the value that maximizes the function

$$\sum_{I \in \mathcal{P}_K} \sum_{j=1}^p \pi_{|I|} \text{BF}(j, I; \sigma^2, \sigma_0^2). \quad (30)$$

In our code, we use the `optimize` function in `R` to solve this one dimensional optimization problem. To estimate σ_{0l}^2 for each $l = 1, \dots, L$, we only need to replace $\mathbf{y}^{(k)}$ by $\tilde{\mathbf{y}}_l^{(k)}$ when we calculate $\text{BF}(j, I; \sigma^2, \sigma_{0l}^2)$ in (30).

B.2 IBSS algorithm is CAVI

In this section, we show that our IBSS algorithm is actually the coordinate ascent variational inference (CAVI) algorithm for maximizing the evidence lower bound (ELBO) over a certain variational family for the muSuSiE model. The main idea of the proof is similar to that for the SuSiE model (see Supplement B of Wang et al. (2020a)).

We begin with a brief review of variational inference. Denote the parameters that we are interested in as $\boldsymbol{\theta}$ and the posterior distribution as $\Pi(\boldsymbol{\theta} | \mathcal{D})$ where \mathcal{D} denotes the data. For any distribution function p and q , let

$$\text{KL}(p \| q) = \int p(\boldsymbol{\theta}) \log \frac{p(\boldsymbol{\theta})}{q(\boldsymbol{\theta})} d\boldsymbol{\theta}$$

be the Kullback–Leibler (KL) divergence between p and q . Let \mathcal{Q} be a density family of $\boldsymbol{\theta}$. The main idea behind variational Bayes is to find some $q \in \mathcal{Q}$ to approximate the posterior distribution $\Pi(\boldsymbol{\theta} | \mathcal{D})$ by minimizing the KL divergence $\text{KL}(q \| \Pi)$. That is, we try to solve the following optimization problem

$$q^* = \arg \min_{q \in \mathcal{Q}} \text{KL}(q \| \Pi(\cdot | \mathcal{D})).$$

Although $\text{KL}(q \| \Pi)$ itself is difficult to evaluate, it can be expressed by using another function which is called evidence lower bound (ELBO) and is much easier to calculate:

$$\text{KL}(q \| p) = \log(P(\mathcal{D})) - \text{ELBO}(q),$$

where

$$\text{ELBO}(q) = \mathbb{E}_q[\log P(\boldsymbol{\theta}, \mathcal{D})] - \mathbb{E}_q[\log q(\boldsymbol{\theta})], \quad (31)$$

where $P(\boldsymbol{\theta}, \mathcal{D}) = P(\boldsymbol{\theta})P(\mathcal{D} | \boldsymbol{\theta})$. Since $P(\mathcal{D})$ does not depend on $\boldsymbol{\theta}$, instead of minimizing the KL divergence, we can aim to find $q \in \mathcal{Q}$ that maximizes the ELBO.

Notice that our muSuSiE model (9) can be considered as a special case of the following additive effects model:

$$\begin{aligned} \mathbf{y}^{(k)} &= \sum_{l=1}^L \boldsymbol{\mu}_l^{(k)} + \mathbf{e}, \text{ where } \mathbf{e} \sim \mathcal{N}(0, \sigma^2 \mathbf{I}) \\ \boldsymbol{\mu}_l &= \left((\boldsymbol{\mu}_l^{(1)})^\top, \dots, (\boldsymbol{\mu}_l^{(K)})^\top \right)^\top \sim g_l, \text{ independently for } l = 1, \dots, L, \end{aligned} \quad (32)$$

where g_l denotes some prior probability distribution. The mean-field variational family we propose to consider is the collection of probability distributions of the form

$$q(\boldsymbol{\mu}_1, \dots, \boldsymbol{\mu}_L) = \prod_{l=1}^L q_l(\boldsymbol{\mu}_l), \quad (33)$$

that is, we let the variational family \mathcal{Q} be the class of distributions on $\boldsymbol{\mu} = (\boldsymbol{\mu}_1, \dots, \boldsymbol{\mu}_L)$ that factorize over $\boldsymbol{\mu}_1, \dots, \boldsymbol{\mu}_L$. Then, the ELBO that we want to optimize becomes

$$\begin{aligned} &\text{ELBO}(q; \sigma^2, (\mathbf{y}^{(k)})_{k \in [K]}) \\ &= \mathbb{E}_q[\log P((\mathbf{y}^{(k)})_{k \in [K]} | \boldsymbol{\mu})] + \mathbb{E}_q\left[\sum_{l=1}^L \log g_l(\boldsymbol{\mu}_l)\right] - \mathbb{E}_q[\log q(\boldsymbol{\mu})] \\ &= -\frac{\sum_{k=1}^K n_k}{2} \log(2\pi\sigma^2) - \frac{1}{2\sigma^2} \sum_{k=1}^K \mathbb{E}_q[\|\mathbf{y}^{(k)} - \sum_{l=1}^L \boldsymbol{\mu}_l^{(k)}\|^2] + \sum_{l=1}^L \mathbb{E}_{q_l} \left[\log \frac{g_l(\boldsymbol{\mu}_l)}{q_l(\boldsymbol{\mu}_l)} \right]. \end{aligned} \quad (34)$$

In the CAVI algorithm (Blei et al., 2017), each step we only update one $\boldsymbol{\mu}_l$ and fix all another $\{\boldsymbol{\mu}_{l'}\}_{l' \neq l}$. For q_l , its ELBO can be expressed by

$$\text{ELBO}(q_l; \sigma^2, (\mathbf{y}^{(k)})_{k \in [K]}) = c - \frac{1}{2\sigma^2} \sum_{k=1}^K \mathbb{E}_{q_l}[\|\tilde{\mathbf{y}}_l^{(k)} - \boldsymbol{\mu}_l\|^2] + \mathbb{E}_{q_l} \left[\log \frac{g_l(\boldsymbol{\mu}_l)}{q_l(\boldsymbol{\mu}_l)} \right],$$

where c is a constant independent of q_l . Because we do not make any constraint on q_l , by the standard result in variational inference (Blei et al., 2017), the distribution which maximizes $\text{ELBO}(q_l; \sigma^2, (\mathbf{y}^{(k)})_{k \in [K]})$ is

$$q_l^*(\boldsymbol{\mu}_l) = \Pi\left(\boldsymbol{\mu}_l | (\tilde{\mathbf{y}}_l^{(k)})_{k \in [K]}\right),$$

where $\Pi(\boldsymbol{\mu}_l | (\tilde{\mathbf{y}}_l^{(k)})_{k \in [K]})$ is the posterior distribution for the model

$$\begin{aligned} \tilde{\mathbf{y}}_l^{(k)} &= \boldsymbol{\mu}_l^{(k)} + \mathbf{e}, \text{ where } \mathbf{e} \sim \mathcal{N}(0, \sigma^2 \mathbf{I}) \\ \boldsymbol{\mu}_l &\sim g_l. \end{aligned} \quad (35)$$

Now consider the muSuSiE model given in (9). By comparing (9) with (32), we see that we can let $\boldsymbol{\mu}_l^{(k)} = \mathbf{X}^{(k)} \boldsymbol{\beta}_l^{(k)}$ and g_l be as described by model (9). Let

$$\boldsymbol{\beta}_l = \left[\boldsymbol{\beta}_l^{(1)}, \dots, \boldsymbol{\beta}_l^{(K)} \right]^\top.$$

Then the variational family we propose becomes

$$q(\beta_1, \dots, \beta_L) = \prod_{l=1}^L q_l(\beta_l).$$

Because we do not make any constraint on q_l , by the CAVI algorithm, we should update q_l by

$$q_l^*(\beta_l) = \Pi(\beta_l | (\tilde{\mathbf{y}}_l)_{k \in [K]}),$$

where $\Pi(\beta_l | (\tilde{\mathbf{y}}_l)_{k \in [K]})$ is the posterior distribution for the muSER model defined in (12) with $\mathbf{y}^{(k)}$ being replaced by $\tilde{\mathbf{y}}_l^{(k)}$. This is exactly how we update β_l in IBSS algorithm; that is, the IBSS algorithm we propose is a CAVI algorithm for muSuSiE.

B.2.1 Estimation of σ^2

We can estimate σ^2 using the value that maximizes the ELBO given in (34). To numerically calculate it, we take partial derivative of (34) with respect to σ^2 and set it to zero, which results in

$$\hat{\sigma}^2 = \frac{\mathbb{E}_q \left[\sum_{k=1}^K \|\mathbf{y}^{(k)} - \sum_{l=1}^L \mu_l^{(k)}\|^2 \right]}{\sum_{k=1}^K n_k}. \quad (36)$$

This can also be seen as a generalization of Equation (B.10) in Wang et al. (2020a) to the multi-task variable selection problem.

B.2.2 Stopping Criterion

We calculate ELBO (34) after updating all L single-effect vectors. If the change in ELBO is less than certain small threshold, we stop the IBSS algorithm; otherwise, we update all L single-effect vectors again.

C More Simulation Results for Variable Selection

The simulation results for $K = 2$ and $\sigma^2 = 1$ or 4 are shown in Table 5, and those for $K = 5$ and $\sigma^2 = 1$ or 4 are shown in Table 6. We make two key observations.

First, as we can see, when the sample size is small ($n = 100$), the multi-task method identifies more activated covariates than the single method, resulting in increased sensitivity and precision. When the sample size increases to 500, the multi-task method improves sensitivity but has a slightly smaller precision, because the multi-tasking approach favors activating covariates simultaneously in two data sets, which can give rise to false positives when some covariate is activated in only one data set but has a very large signal size.

Second, when all the other parameters are fixed, the multi-task method on five data sets outperforms the multi-task method on two data sets, with the former significantly improving both sensitivity and precision. This is evident when n is small. When n is large, the advantage of the multi-task method on five data sets over on two data sets is still noticeable (especially when $\sigma^2 = 4$) but less significant.

p	n	$ s_1^* $	$ s_2^* $	σ^2	sens_mu	sens_si	prec_mu	prec_si
600	100	10	2	1	0.4526	0.2632	0.9884	0.9365
600	100	10	5	1	0.3456	0.2045	0.9747	0.9258
600	100	25	2	1	0.1259	0.0656	0.9408	0.7608
600	100	25	5	1	0.089	0.0499	0.8976	0.7229
600	100	10	2	4	0.1233	0.0656	0.7694	0.5547
600	100	10	5	4	0.0931	0.0521	0.7576	0.5482
600	100	25	2	4	0.0499	0.024	0.7389	0.4605
600	100	25	5	4	0.0364	0.0187	0.6643	0.4184
1000	500	10	2	1	0.8121	0.7063	0.9962	1
1000	500	10	5	1	0.7905	0.7011	0.9928	0.9996
1000	500	25	2	1	0.8191	0.696	0.9985	1
1000	500	25	5	1	0.804	0.6949	0.9964	0.9999
1000	500	10	2	4	0.613	0.4655	0.9945	0.9987
1000	500	10	5	4	0.5735	0.4549	0.9901	0.9997
1000	500	25	2	4	0.6077	0.4389	0.9978	0.9999
1000	500	25	5	4	0.577	0.4332	0.9951	0.9997

Table 5: Simulation results for two data sets. For each setting, the result is averaged over 500 replicates.

p	n	$ s_1^* $	$ s_2^* $	σ^2	sens_mu	sens_si	prec_mu	prec_si
600	100	10	2	1	0.5976	0.2551	0.9907	0.9328
600	100	10	5	1	0.495	0.2007	0.9795	0.9269
600	100	25	2	1	0.3344	0.066	0.9877	0.7662
600	100	25	5	1	0.1635	0.0501	0.9655	0.7161
600	100	10	2	4	0.2263	0.0657	0.9408	0.5503
600	100	10	5	4	0.1495	0.0511	0.8889	0.539
600	100	25	2	4	0.0859	0.0241	0.8875	0.4687
600	100	25	5	4	0.0611	0.02037	0.8263	0.4428
1000	500	10	2	1	0.8181	0.7062	0.9936	0.9999
1000	500	10	5	1	0.7921	0.7025	0.9887	0.9998
1000	500	25	2	1	0.8261	0.6927	0.9974	0.9999
1000	500	25	5	1	0.8101	0.6916	0.9938	0.9999
1000	500	10	2	4	0.6641	0.4593	0.992	0.9993
1000	500	10	5	4	0.6167	0.454	0.9865	0.9996
1000	500	25	2	4	0.6776	0.4362	0.9967	0.9998
1000	500	25	5	4	0.6503	0.4301	0.9935	0.9998

Table 6: Simulation results for five data sets. For each setting, the result is averaged over 500 replicates.

prior	$p^{-\omega_1}$	$p^{-\omega_2}$
prior 1	$p^{-1.25}/2$	$p^{-1.5}$
prior 2	$p^{-1.5}/2$	p^{-2}
prior 3	p^{-2}	$p^{-2.25}$
prior 4	$p^{-2}/2$	$p^{-2.25}$

Table 7: Prior hyperparameters for muSuSiE-DAG for $K = 2$.

prior	$p^{-\omega_1}$	$p^{-\omega_2}$	$p^{-\omega_3}$	$p^{-\omega_4}$	$p^{-\omega_5}$
prior 1	$p^{-1.5}/5$	$p^{-1.75}/10$	$p^{-2}/10$	$p^{-2.25}/5$	$p^{-2.5}$
prior 2	$p^{-1.75}$	p^{-2}	$p^{-2.25}$	$p^{-2.5}$	p^{-3}
prior 3	$p^{-1.75}/5$	$p^{-2}/10$	$p^{-2.25}/10$	$p^{-2.5}/5$	p^{-3}
prior 4	p^{-2}	$p^{-2.25}$	$p^{-2.5}$	$p^{-2.75}$	p^{-3}

Table 8: Prior hyperparameters for muSuSiE-DAG for $K = 5$.

D More Simulation Results for Differential DAG Analysis

Recall that we use simulation studies to compare the performance of four methods for joint estimation of multiple DAG models: PC, GES, joint GES, and muSuSiE-DAG. We use N_{com} to denote the number of shared edges and N_{pri} to denote the number of edges unique to each data set. In each simulation setting, we report the average number of wrong edges N_{wrong} , the average true positive (TP) rate and the average false positive (FP) rate by ignoring edge directions. In addition, we introduce the fourth measurement metric, the squared Frobenius Norm (F-norm) between the true adjacency matrix and estimated adjacency matrix, which can be calculated as follows. For PC, GES and joint GES method, we let $\hat{\mathbf{R}}^{(k)} \in \{0, 1\}^{p \times p}$ be the estimated adjacency matrix such that $\hat{R}_{ij}^{(k)} = 1$ if the edge (i, j) is in the estimated DAG for the k -th data set and $\hat{R}_{ij}^{(k)} = 0$ otherwise. For muSuSiE-DAG, we let $\hat{\mathbf{R}}^{(k)}$ be as defined in (20) where each entry is the estimated probability of the edge and thus takes value in $[0, 1]$. Let $\{\mathbf{R}^{(k)}\}_{k=1}^K$ be the true adjacency matrices where $R_{ij}^{(k)} = 1$ if the (i, j) is in the k -th true DAG model and $R_{ij}^{(k)} = 0$ otherwise. For each method, the F-norm metric is defined as

$$\sum_{i=1}^{p-1} \sum_{j=i+1}^p \left(\hat{R}_{ij}^{(k)} + \hat{R}_{ji}^{(k)} - R_{ij}^{(k)} - R_{ji}^{(k)} \right)^2.$$

For PC, GES and joint GES, this is equivalent to counting the number of wrong edges. But for muSuSiE-DAG, this statistic in general is different from N_{wrong} . Table 10 shows the results for the PC method, Table 11 for GES and Table 12 for joint GES. Note that the values of the tuning parameters are also given in the corresponding tables, including the significance level α for the PC method, and l_0 -penalization parameter λ for GES and joint GES. For muSuSiE-DAG, the choice of the parameters $\omega_1, \dots, \omega_K$ is detailed in Table 7 (for $K = 2$) and Table 8 (for $K = 5$). Table 13 shows the results for our muSuSiEDAG method. Table 9 compares results for all methods when $K = 5$, where for each method we use the optimal tuning parameter.

As expected, joint methods, joint GES and muSuSiEDAG, have much larger true positive rates

method	K	N_{com}	N_{pri}	N_{wrong}	TP	FP
PC	5	100	20	31.844	0.7504	4e-04
GES	5	100	20	23.108	0.8178	3e-04
joint GES	5	100	20	23.084	0.8888	0.002
muSuSiE-DAG	5	100	20	16.612	0.9071	0.0011
PC	5	100	50	43.904	0.7044	3e-04
GES	5	100	50	30.196	0.8157	5e-4
joint GES	5	100	50	35.648	0.8599	0.003
muSuSiE-DAG	5	100	50	28.572	0.8756	0.002
PC	5	50	50	25.116	0.7309	1e-04
GES	5	50	50	19.288	0.8166	2e-04
joint GES	5	50	50	33.292	0.8479	0.0037
muSuSiE-DAG	5	50	50	18.488	0.8522	8e-04

Table 9: Simulation results for joint estimation of multiple DAG models with $K = 5$.

and slightly larger false positive rates than the two single-analysis methods, PC and GES. This is because the joint method can identify edges with low signal strength if it is expressed concurrently in all K data sets, which leads to a higher true positive rate, while the joint method may also identify edges with extremely high signal strength in a single data set as expressed simultaneously in more than one data sets, resulting in a higher false positive rate. Additionally, when the ratio $N_{\text{com}}/N_{\text{pri}}$ is large, implying that the majority of edges are shared, the joint method outperforms the other two by a large margin. When the ratio $N_{\text{com}}/N_{\text{pri}}$ is small, GES may even outperform joint GES. In all cases, our muSuSiE-DAG method has the best performance in terms of the metric N_{wrong} . We also observe that the results may depend on the choice of the prior parameters (though not significantly), which suggests that in reality one may want to tune the parameters to improve the performance of the algorithm.

E Additional results for real data analysis

Table 14 shows additional results for the real data example presented in Section 6 with other choices of the tuning parameters. Results for PC, GES and joint GES methods combined with stability selection (Meinshausen and Bühlmann, 2010), which we implemented using `stabselect` function in the `stabs` package, are shown in Table 15. There is a hyperparameter `cutoff` in `stabselect` function, which we denote by “cutoff1” in the table. The `stabselect` function returns a selection probability for each edge, and as a result, we need to choose a threshold, denoted by “cutoff2”, to obtain a DAG from the stable selection result. In Table 15, we list the results for cutoff1 = 0.6, 0.7, 0.8, 0.9 and cutoff2 = 0.55, 0.75.

References

Raj Agrawal, Caroline Uhler, and Tamara Broderick. Minimal I-MAP MCMC for scalable structure discovery in causal DAG models. In *International Conference on Machine Learning*, pages 89–98, 2018.

K	α	N_{com}	N_{pri}	N_{wrong}	TP	FP	F-norm
2	1e-04	100	20	38.52	0.68	0	38.52
2	5e-04	100	20	34.1	0.7183	1e-04	34.1
2	0.001	100	20	32.04	0.7373	1e-04	32.04
2	0.005	100	20	28.29	0.7822	4e-04	28.29
2	0.01	100	20	28.55	0.8009	0.001	28.55
2	0.05	100	20	45.83	0.8523	0.0058	45.83
2	1e-04	100	50	54.04	0.6404	0	54.04
2	5e-04	100	50	47.93	0.6823	1e-04	47.93
2	0.001	100	50	45.32	0.7007	1e-04	45.32
2	0.005	100	50	39.37	0.7475	3e-04	39.37
2	0.01	100	50	37.93	0.7674	6e-04	37.93
2	0.05	100	50	44.9	0.8225	0.0038	44.9
2	1e-04	50	50	28.13	0.7192	0	28.13
2	5e-04	50	50	24.59	0.7572	1e-04	24.59
2	0.001	50	50	23.44	0.7723	1e-04	23.44
2	0.005	50	50	21.9	0.8121	6e-04	21.9
2	0.01	50	50	23.34	0.8312	0.0013	23.34
2	0.05	50	50	47.78	0.8796	0.0073	47.78
5	1e-04	100	20	43.108	0.6413	0	43.108
5	5e-04	100	20	38.428	0.6816	0	38.428
5	0.001	100	20	36.264	0.701	1e-04	36.264
5	0.005	100	20	32.044	0.7504	4e-04	32.044
5	0.01	100	20	31.844	0.7725	9e-04	31.844
5	0.05	100	20	47.924	0.8286	0.0056	47.924
5	1e-04	100	50	62.304	0.5854	0	62.304
5	5e-04	100	50	55.508	0.6313	0	55.508
5	0.001	100	50	52.528	0.6521	1e-04	52.528
5	0.005	100	50	45.78	0.7044	3e-04	45.78
5	0.01	100	50	43.904	0.7276	6e-04	43.904
5	0.05	100	50	50.608	0.7897	0.0039	50.608
5	1e-04	50	50	33	0.6703	0	33
5	5e-04	50	50	29.064	0.7114	0	29.064
5	0.001	50	50	27.424	0.7309	1e-04	27.424
5	0.005	50	50	25.116	0.779	6e-04	25.116
5	0.01	50	50	26.036	0.8002	0.0012	26.036
5	0.05	50	50	49.848	0.8535	0.0072	49.848

Table 10: Simulation results for the PC algorithm. N_{wrong} is the same as F-norm by definition.

K	λ	N_{com}	N_{pri}	N_{wrong}	TP	FP	F-norm
2	1	100	20	32.47	0.9152	0.0046	32.47
2	2	100	20	19.67	0.8482	3e-04	19.67
2	3	100	20	26.76	0.7837	2e-04	26.76
2	4	100	20	33.26	0.7269	1e-04	33.26
2	5	100	20	39.03	0.6777	1e-04	39.03
2	1	100	50	35.26	0.9191	0.0048	35.26
2	2	100	50	24.84	0.8505	5e-04	24.84
2	3	100	50	33.12	0.7895	3e-04	33.12
2	4	100	50	40.31	0.7383	2e-04	40.31
2	5	100	50	47.35	0.6893	2e-04	47.35
2	1	50	50	29	0.9223	0.0043	29
2	2	50	50	15.74	0.8514	2e-04	15.74
2	3	50	50	21.15	0.7925	1e-04	21.15
2	4	50	50	26.47	0.7374	0	26.47
2	5	50	50	31.16	0.6904	0	31.16
5	1	100	20	35.548	0.8955	0.0047	35.548
5	2	100	20	23.108	0.8178	3e-04	23.108
5	3	100	20	31.008	0.7466	1e-04	31.008
5	4	100	20	38.44	0.6824	1e-04	38.44
5	5	100	20	46.012	0.6184	0	46.012
5	1	100	50	40.36	0.8953	0.0051	40.36
5	2	100	50	30.196	0.8157	5e-04	30.196
5	3	100	50	39.664	0.744	3e-04	39.664
5	4	100	50	48.988	0.6791	2e-04	48.988
5	5	100	50	58.332	0.615	1e-04	58.332
5	1	50	50	32.58	0.8976	0.0046	32.58
5	2	50	50	19.288	0.8166	2e-04	19.288
5	3	50	50	25.852	0.7453	1e-04	25.852
5	4	50	50	32.2	0.68	0	32.2
5	5	50	50	38.18	0.6195	0	38.18

Table 11: Simulation results for the GES method. N_{wrong} is the same as F-norm by definition.

K	λ	N_{com}	N_{pri}	N_{wrong}	TP	FP	F-norm
2	1	100	20	38.96	0.9176	0.006	38.96
2	2	100	20	15.5	0.9117	0.001	15.5
2	3	100	20	16.58	0.8948	8e-04	16.58
2	4	100	20	18.48	0.8754	7e-04	18.48
2	5	100	20	20.7	0.8552	7e-04	20.7
2	1	100	50	47.13	0.9177	0.0072	47.13
2	2	100	50	24.94	0.9003	0.0021	24.94
2	3	100	50	25.69	0.8787	0.0015	25.69
2	4	100	50	28.67	0.8556	0.0014	28.67
2	5	100	50	32.08	0.8295	0.0013	32.08
2	1	50	50	39.19	0.9022	0.006	39.19
2	2	50	50	23.11	0.8836	0.0023	23.11
2	3	50	50	24.72	0.8535	0.0021	24.72
2	4	50	50	27.83	0.818	0.002	27.83
2	5	50	50	30.77	0.786	0.0019	30.77
5	1	100	20	75.172	0.8946	0.0128	75.172
5	2	100	20	26.868	0.894	0.0029	26.868
5	3	100	20	23.084	0.8888	0.002	23.084
5	4	100	20	23.968	0.878	0.0019	23.968
5	5	100	20	24.728	0.8693	0.0019	24.728
5	1	100	50	90.5	0.8974	0.0155	90.5
5	2	100	50	36.244	0.8797	0.0038	36.244
5	3	100	50	35.648	0.8599	0.003	35.648
5	4	100	50	38.22	0.8403	0.0029	38.22
5	5	100	50	40.552	0.8218	0.0028	40.552
5	1	50	50	71.296	0.8718	0.0119	71.296
5	2	50	50	33.292	0.8479	0.0037	33.292
5	3	50	50	33.712	0.8204	0.0032	33.712
5	4	50	50	36.48	0.7921	0.0032	36.48
5	5	50	50	39.86	0.7622	0.0033	39.86

Table 12: Simulation results for the joint GES method. N_{wrong} is the same as F-norm by definition.

K	prior	N_{com}	N_{pri}	N_{wrong}	TP	FP	F-norm
2	prior 1	100	20	18.32	0.9245	0.0019	16.4796
2	prior 2	100	20	14.81	0.9058	7e-04	12.6889
2	prior 3	100	20	13.23	0.9066	4e-04	11.1563
2	prior 4	100	20	12.95	0.9138	5e-04	11.1728
2	prior 1	100	50	26.55	0.9125	0.0028	24.4017
2	prior 2	100	50	19.73	0.8989	9e-04	17.2663
2	prior 3	100	50	19.23	0.8945	7e-04	16.919
2	prior 4	100	50	18.93	0.8988	8e-04	16.8877
2	prior 1	50	50	18.07	0.8982	0.0016	16.7013
2	prior 2	50	50	14.77	0.8816	6e-04	13.1345
2	prior 3	50	50	14.83	0.874	5e-04	13.1556
2	prior 4	50	50	15.05	0.877	6e-04	13.5774
5	prior 1	100	20	17.864	0.9259	0.0018	15.2454
5	prior 2	100	20	26.408	0.881	0.0025	23.3181
5	prior 3	100	20	16.612	0.9071	0.0011	13.9164
5	prior 4	100	20	18.848	0.8985	0.0014	16.1615
5	prior 1	100	50	31.476	0.8904	0.0031	27.9713
5	prior 2	100	50	42.908	0.8519	0.0043	38.7376
5	prior 3	100	50	28.572	0.8756	0.002	25.1541
5	prior 4	100	50	32.504	0.8683	0.0026	28.8933
5	prior 1	50	50	19.536	0.868	0.0013	17.5978
5	prior 2	50	50	25.64	0.8422	0.002	23.5666
5	prior 3	50	50	18.488	0.8522	8e-04	16.3749
5	prior 4	50	50	20.856	0.8504	0.0012	18.8697

Table 13: Simulation results for the muSuSiE-DAG method.

Method	Parameters	$ \mathcal{G}_1 $	$ \mathcal{G}_2 $	$ \mathcal{G}_1 \cap \mathcal{G}_2 $	N_{total}	ratio
PC	$\alpha = 1e - 04$	12	26	7	31	0.2258
PC	$\alpha = 5e - 04$	19	38	13	44	0.2955
PC	$\alpha = 0.001$	23	39	14	48	0.2917
PC	$\alpha = 0.005$	33	60	18	75	0.24
PC	$\alpha = 0.01$	42	69	19	92	0.2065
PC	$\alpha = 0.05$	73	109	24	158	0.1519
GES	$\lambda = 1$	150	238	49	339	0.1445
GES	$\lambda = 2$	99	148	43	204	0.2108
GES	$\lambda = 3$	78	108	34	152	0.2237
GES	$\lambda = 4$	75	92	32	135	0.237
GES	$\lambda = 5$	75	87	31	131	0.2366
joint GES	$\lambda = 1$	73	80	58	95	0.6105
joint GES	$\lambda = 2$	64	68	59	73	0.8082
joint GES	$\lambda = 3$	51	54	49	56	0.875
joint GES	$\lambda = 4$	38	41	36	43	0.8372
joint GES	$\lambda = 5$	31	33	31	33	0.9394
muSuSiE-DAG	$p^{-\omega_1} = p^{-1.25}, p^{-\omega_2} = p^{-2}$	33	112	28	117	0.2393
muSuSiE-DAG	$p^{-\omega_1} = p^{-1.5}, p^{-\omega_2} = p^{-2.5}$	28	98	26	100	0.26
muSuSiE-DAG	$p^{-\omega_1} = p^{-1.5}/2, p^{-\omega_2} = p^{-2}$	42	92	41	93	0.4409
muSuSiE-DAG	$p^{-\omega_1} = p^{-2}, p^{-\omega_2} = p^{-3.5}$	17	68	15	70	0.2143
muSuSiE-DAG	$p^{-\omega_1} = p^{-2}/2, p^{-\omega_2} = p^{-3.5}$	22	71	21	72	0.2917
muSuSiE-DAG	$p^{-\omega_1} = p^{-\omega_2} = p^{-2}$	56	83	56	83	0.6747

Table 14: More results for the real data analysis. $|\mathcal{G}_k|$: number of edges in the estimated DAG for the k -th group; $|\mathcal{G}_1 \cap \mathcal{G}_2|$: number of edges shared by both DAGs; N_{total} : total number of edges in two DAGs; ratio: the ratio of $|\mathcal{G}_1 \cap \mathcal{G}_2|$ to N_{total} .

Method	cutoff1	cutoff2	$ \mathcal{G}_1 $	$ \mathcal{G}_2 $	$ \mathcal{G}_1 \cap \mathcal{G}_2 $	N_{total}	ratio
PC	0.6	0.55	51	90	19	122	0.1557
PC	0.6	0.75	36	64	18	82	0.2195
PC	0.7	0.55	48	85	19	114	0.1667
PC	0.7	0.75	33	59	18	74	0.2432
PC	0.8	0.55	53	82	20	115	0.1739
PC	0.8	0.75	37	60	19	78	0.2436
PC	0.9	0.55	50	85	19	116	0.1638
PC	0.9	0.75	36	61	18	79	0.2278
GES	0.6	0.55	102	149	43	208	0.2067
GES	0.6	0.75	70	103	33	140	0.2357
GES	0.7	0.55	100	160	43	217	0.1982
GES	0.7	0.75	70	96	33	133	0.2481
GES	0.8	0.55	98	155	44	209	0.2105
GES	0.8	0.75	70	97	34	133	0.2556
GES	0.9	0.55	98	156	41	213	0.1925
GES	0.9	0.75	66	96	30	132	0.2273
joint GES	0.6	0.55	60	62	57	65	0.8769
joint GES	0.6	0.75	45	45	43	47	0.9149
joint GES	0.7	0.55	60	63	49	74	0.6622
joint GES	0.7	0.75	54	54	52	56	0.9286
joint GES	0.8	0.55	60	62	56	66	0.8485
joint GES	0.8	0.75	42	46	41	47	0.8723
joint GES	0.9	0.55	58	63	50	71	0.7042
joint GES	0.9	0.75	50	50	48	52	0.9231

Table 15: More results for PC, GES and joint GES methods in the real data analysis. $|\mathcal{G}_k|$: number of edges in the estimated DAG for the k -th group; $|\mathcal{G}_1 \cap \mathcal{G}_2|$: number of edges shared by both DAGs; N_{total} : total number of edges in two DAGs; ratio: the ratio of $|\mathcal{G}_1 \cap \mathcal{G}_2|$ to N_{total} .

- David M Blei, Alp Kucukelbir, and Jon D McAuliffe. Variational inference: A review for statisticians. *Journal of the American Statistical Association*, 112(518):859–877, 2017.
- Edwin V Bonilla, Kian Chai, and Christopher Williams. Multi-task Gaussian process prediction. *Advances in Neural Information Processing Systems*, 20, 2007.
- Xinshi Chen, Haoran Sun, Caleb Ellington, Eric Xing, and Le Song. Multi-task learning of order-consistent causal graphs. *Advances in Neural Information Processing Systems*, 34, 2021.
- David Maxwell Chickering. Optimal structure identification with greedy search. *Journal of Machine Learning Research*, 3(Nov):507–554, 2002.
- Patrick Danaher, Pei Wang, and Daniela M Witten. The joint graphical lasso for inverse covariance estimation across multiple classes. *Journal of the Royal Statistical Society: Series B (Statistical Methodology)*, 76(2):373–397, 2014.
- Mark WEJ Fiers, Liesbeth Minnoye, Sara Aibar, Carmen Bravo González-Blas, Zeynep Kalender Atak, and Stein Aerts. Mapping gene regulatory networks from single-cell omics data. *Briefings in functional genomics*, 17(4):246–254, 2018.
- Eva-Maria Fronk and Paolo Giudici. Markov Chain Monte Carlo model selection for DAG models. *Statistical Methods and Applications*, 13(3):259–273, 2004.
- Edward I George and Robert E McCulloch. Variable selection via Gibbs sampling. *Journal of the American Statistical Association*, 88(423):881–889, 1993.
- Asish Ghoshal, Kevin Bello, and Jean Honorio. Direct learning with guarantees of the difference DAG between structural equation models. *arXiv preprint arXiv:1906.12024*, 2019.
- André R Gonçalves, Fernando J Von Zuben, and Arindam Banerjee. Multi-task sparse structure learning with gaussian copula models. *The Journal of Machine Learning Research*, 17(1):1205–1234, 2016.
- Shengbo Guo, Onno Zoeter, and Cédric Archambeau. Sparse Bayesian multi-task learning. *Advances in Neural Information Processing Systems*, 24, 2011.
- Naftali Harris and Mathias Drton. PC algorithm for nonparanormal graphical models. *Journal of Machine Learning Research*, 14(11), 2013.
- Daniel Hernández-Lobato, José Miguel Hernández-Lobato, and Zoubin Ghahramani. A probabilistic model for dirty multi-task feature selection. In *International Conference on Machine Learning*, pages 1073–1082. PMLR, 2015.
- Hemant Ishwaran and J Sunil Rao. Spike and slab variable selection: Frequentist and Bayesian strategies. *The Annals of Statistics*, 33(2):730–773, 2005.
- Ali Jalali, Sujay Sanghavi, Chao Ruan, and Pradeep Ravikumar. A dirty model for multi-task learning. *Advances in Neural Information Processing Systems*, 23, 2010.
- Seonghyun Jeong and Subhashis Ghosal. Unified bayesian theory of sparse linear regression with nuisance parameters. *Electronic Journal of Statistics*, 15(1):3040–3111, 2021.

- Wenxin Jiang and Martin A Tanner. Gibbs posterior for variable selection in high-dimensional classification and data mining. *The Annals of Statistics*, 36(5):2207–2231, 2008.
- Valen E Johnson and David Rossell. Bayesian model selection in high-dimensional settings. *Journal of the American Statistical Association*, 107(498):649–660, 2012.
- Markus Kalisch, Martin Mächler, Diego Colombo, Marloes H Maathuis, and Peter Bühlmann. Causal inference using graphical models with the R package pcalg. *Journal of Statistical Software*, 47:1–26, 2012.
- Minoru Kanehisa, Susumu Goto, Yoko Sato, Miho Furumichi, and Mao Tanabe. KEGG for integration and interpretation of large-scale molecular data sets. *Nucleic Acids Research*, 40(D1):D109–D114, 2012.
- Daphne Koller and Nir Friedman. *Probabilistic graphical models: Principles and techniques*. MIT press, 2009.
- Jack Kuipers and Giusi Moffa. Partition MCMC for inference on acyclic digraphs. *Journal of the American Statistical Association*, 112(517):282–299, 2017.
- Jack Kuipers, Polina Suter, and Giusi Moffa. Efficient sampling and structure learning of Bayesian networks. *Journal of Computational and Graphical Statistics*, pages 1–12, 2022.
- Yan Li, Dayou Liu, Tengfei Li, and Yungang Zhu. Bayesian differential analysis of gene regulatory networks exploiting genetic perturbations. *BMC Bioinformatics*, 21(1):1–13, 2020.
- Karim Lounici, Massimiliano Pontil, Alexandre B Tsybakov, and Sara Van De Geer. Taking advantage of sparsity in multi-task learning. *arXiv preprint arXiv:0903.1468*, 2009.
- Karim Lounici, Massimiliano Pontil, Sara Van De Geer, and Alexandre B Tsybakov. Oracle inequalities and optimal inference under group sparsity. *The Annals of Statistics*, 39(4):2164–2204, 2011.
- Nicolai Meinshausen and Peter Bühlmann. Stability selection. *Journal of the Royal Statistical Society: Series B (Statistical Methodology)*, 72(4):417–473, 2010.
- Preetam Nandy, Alain Hauser, and Marloes H Maathuis. High-dimensional consistency in score-based and hybrid structure learning. *The Annals of Statistics*, 46(6A):3151–3183, 2018.
- Naveen Naidu Narisetty and Xuming He. Bayesian variable selection with shrinking and diffusing priors. *The Annals of Statistics*, 42(2):789–817, 2014.
- Xiangyu Niu, Yifan Sun, and Jinyuan Sun. Latent group structured multi-task learning. In *2018 52nd Asilomar Conference on Signals, Systems, and Computers*, pages 850–854. IEEE, 2018.
- Diane Oyen and Terran Lane. Leveraging domain knowledge in multitask Bayesian network structure learning. In *Twenty-Sixth AAAI Conference on Artificial Intelligence*, 2012.
- Christine Peterson, Francesco C Stingo, and Marina Vannucci. Bayesian inference of multiple Gaussian graphical models. *Journal of the American Statistical Association*, 110(509):159–174, 2015.

- Christine B Peterson and Francesco C Stingo. Bayesian estimation of single and multiple graphs. In *Handbook of Bayesian Variable Selection*, pages 327–348. Chapman and Hall/CRC, 2021.
- Christine B Peterson, Nathan Osborne, Francesco C Stingo, Pierrick Bourgeat, James D Doecke, and Marina Vannucci. Bayesian modeling of multiple structural connectivity networks during the progression of Alzheimer’s disease. *Biometrics*, 76(4):1120–1132, 2020.
- Kolyan Ray and Botond Szabó. Variational Bayes for high-dimensional linear regression with sparse priors. *Journal of the American Statistical Association*, pages 1–12, 2021.
- Elin Shaddox, Christine B Peterson, Francesco C Stingo, Nicola A Hanania, Charmion Cruickshank-Quinn, Katerina Kechris, Russell Bowler, and Marina Vannucci. Bayesian inference of networks across multiple sample groups and data types. *Biostatistics*, 21(3):561–576, 2020.
- Ali Shojaie. Differential network analysis: A statistical perspective. *Wiley Interdisciplinary Reviews: Computational Statistics*, 13(2):e1508, 2021.
- Peter Spirtes, Clark N Glymour, Richard Scheines, and David Heckerman. *Causation, prediction, and search*. MIT press, 2000.
- Richard W Tothill, Anna V Tinker, Joshy George, Robert Brown, Stephen B Fox, Stephen Lade, Daryl S Johnson, Melanie K Trivett, Dariush Etemadmoghadam, Bianca Locandro, et al. Novel molecular subtypes of serous and endometrioid ovarian cancer linked to clinical outcome. *Clinical cancer research*, 14(16):5198–5208, 2008.
- Bram Van de Sande, Christopher Flerin, Kristofer Davie, Maxime De Waegeneer, Gert Hulselmans, Sara Aibar, Ruth Seurinck, Wouter Saelens, Robrecht Cannoodt, Quentin Rouchon, Toni Verbeiren, Dries De Maeyer, Joke Reumers, Yvan Saeys, and Stein Aerts. A scalable SCENIC workflow for single-cell gene regulatory network analysis. *Nature Protocols*, 15(7):2247–2276, 2020.
- Gao Wang, Abhishek Sarkar, Peter Carbonetto, and Matthew Stephens. A simple new approach to variable selection in regression, with application to genetic fine mapping. *Journal of the Royal Statistical Society: Series B (Statistical Methodology)*, 82(5):1273–1300, 2020a.
- Yuhao Wang, Santiago Segarra, and Caroline Uhler. High-dimensional joint estimation of multiple directed Gaussian graphical models. *Electronic Journal of Statistics*, 14(1):2439–2483, 2020b.
- Masanao Yajima, Donatello Telesca, Yuan Ji, and Peter Müller. Detecting differential patterns of interaction in molecular pathways. *Biostatistics*, 16(2):240–251, 2015.
- Yun Yang, Martin J Wainwright, and Michael I Jordan. On the computational complexity of high-dimensional Bayesian variable selection. *The Annals of Statistics*, 44(6):2497–2532, 2016.
- Yu Zhang and Qiang Yang. A survey on multi-task learning. *IEEE Transactions on Knowledge and Data Engineering*, 2021.